J. Fluid Mech. (1988), *vol.* 194, *pp.* 417–456
Printed in Great Britain

Instability and transition in curved channel flow

By W. H. FINLAY†, J. B. KELLER‡ AND J. H. FERZIGER‡

† Department of Mechanical Engineering, University of Alberta, Edmonton, Alberta, Canada T6G 2G8

‡ Department of Mechanical Engineering, Stanford University, Stanford, CA 94305, USA

(Received 16 June 1987 and in revised form 26 January 1988)

A theoretical and numerical investigation of streamwise-oriented Dean vortices in curved channel flow is presented. The principal results are obtained from three-dimensional pseudospectral simulations of the incompressible time-dependent Navier–Stokes equations. With increasing Reynolds number, a sequence of transitions similar to that observed in non-turbulent Taylor–Couette flow is found. The transition from laminar curved channel Poiseuille flow to axisymmetric Dean vortex flow is studied using linear and weakly nonlinear analyses; these results are compared to the full simulations. Using the code, two transitions that cause the axisymmetric vortices to develop waves travelling in the streamwise direction at higher Reynolds numbers are discovered. The linear stability of axisymmetric Dean vortex flow to non-axisymmetric perturbations is examined. Associated with the two transitions are two different non-axisymmetric flows: undulating and twisting Dean vortex flow. Undulating vortices are similar to wavy Taylor vortices. Twisting vortices, with a much shorter streamwise wavelength, are dissimilar; to our knowledge, they have no counterpart in the Taylor–Couette problem. At sufficiently high Reynolds numbers, linear growth rates associated with twisting vortices far exceed those associated with undulating vortices. For the channel curvatures studied, angular speeds of both kinds of travelling waves are only weakly dependent on Reynolds number and wavenumber. A bifurcation limits the vortex spacings that can be examined and suggests an Eckhaus stability boundary. The development of wavy vortex flows from small-amplitude disturbances shows that full development of undulating vortices may require a streamwise distance greater than one circumference, whereas for sufficiently large Reynolds numbers, twisting vortices reach equilibrium amplitude within half this distance and are therefore more likely to be observed experimentally. We suggest twisting vortices are due to a shear instability.

1. Introduction

This work uses analytical and numerical techniques to study curved channel flow instabilities. Understanding the transitions that curved channel flow undergoes may yield a better understanding of the physics of transition in general, and in other curved geometries in particular.

The flow geometry is shown in figure 1. The inner and outer walls of the channel have radii of curvature r_i and r_o respectively, and the channel centreline radius is r_c. The channel spacing is $d = r_o - r_i$. A non-dimensional measure of the channel curvature is the radius ratio $\eta = r_i/r_o$. Throughout this work, velocities and lengths will be non-dimensionalized by the mean streamwise velocity $\bar{U}$ and $\frac{1}{2}d$, respectively. We define a Reynolds number $Re = \bar{U}d/2\nu$. The cylindrical coordinate system is

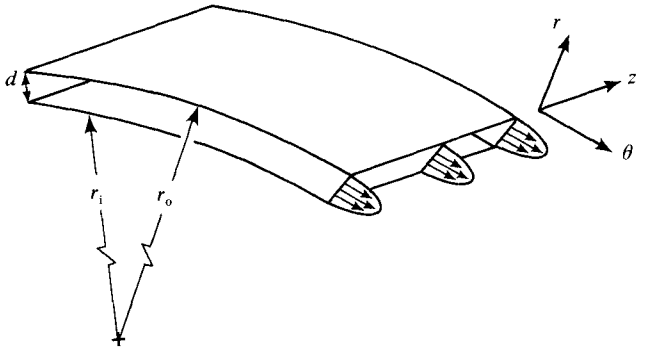

FIGURE 1. The curved channel flow geometry.

aligned such that (r, θ, z) are the normal, streamwise, and spanwise directions respectively. Curved channel flow experiments have streamwise extent less than 2π rad if r_c is fixed and have finite aspect ratio $\Gamma = h/d$, where h is the spanwise dimension of the channel.

At sufficiently small Re, the velocity in infinite-span curved channel flow is purely streamwise. Its profile is similar to the parabolic profile of plane channel flow, but the location of maximum velocity is shifted towards the outer wall. We call this flow 'curved channel Poiseuille flow' (CCPF). At higher Re, centrifugal instability causes a secondary flow containing streamwise-oriented Dean vortices similar to the Taylor vortices of Taylor–Couette flow. Dean vortices occur in regularly spaced counter-rotating pairs. (Finite span and other effects may cause uneven spacing.) We define a non-dimensional spanwise wavenumber of the vortices as $a = \pi d/\lambda$, where λ is the spanwise vortex spacing.

For given η and a, linear neutral stability analysis predicts the neutrally stable Reynolds number, $Re_{ns}(a)$, above which axisymmetric Dean vortices have positive linear growth rates. For fixed η, this result is a neutral stability curve $Re_{ns}(a)$. Dean (1928) used a narrow-gap approximation ($\eta \sim 1$) and found the minimum of the neutral stability curve, which occurs at the critical Reynolds number Re_c and critical wavenumber a_c. CCPF occurs for $Re < Re_c$; Dean vortices occur for $Re > Re_c$. (Re_c is singular for $\eta = 1$, so the Dean number $De = 2Re(d/r_i)^{\frac{1}{2}}$ is used in the narrow-gap case, for which $De_c = 35.92$.) For the narrow-gap case, Reid (1958) and Hammerlin (1958) determined part of the neutral stability curve for a near a_c. For $\eta = 0.923$, the experiment of Brewster, Grosberg & Nissan (1959) confirmed the existence of a critical Reynolds number Re_c above which steady Dean vortices develop. Sparrow (1964) and Walowit, Tsao & DiPrima (1964) examined the linear neutral stability of wide-gap Dean vortices, confirming the value of Re_c found experimentally by Brewster *et al.* (1959).

For $\eta \geqslant 0.95$, Gibson & Cook (1974) examined the linear neutral stability of CCPF to infinitesimal non-axisymmetric disturbances with spatial dependence of the form $f(r)\, e^{iaz}\, e^{i\beta\theta}$. Axisymmetric disturbances have $\beta = 0$, $a \neq 0$, two-dimensional Tollmien–Schlichting (TS) waves have $a = 0$, $\beta \neq 0$, and mixed modes have $a \neq 0$, $\beta \neq 0$. For $\eta = 1$, Squires theorem (Drazin & Reid 1981) indicates that for each unstable mixed mode there is a more unstable two-dimensional TS wave. Gibson & Cook (1974) showed that this result also holds for narrow-gap curved channels, so it is only necessary to consider two-dimensional TS and axisymmetric modes. They found that when $0.95 \leqslant \eta < (1 - 2.179 \times 10^{-5})$, axisymmetric disturbances are more unstable

than two-dimensional TS modes, but for $\eta > (1-2.179\times10^{-5})$ the reverse is true. For wide gaps, Jankowski & Takeuchi (1976) indicate that axisymmetric disturbances are the most unstable. Daudpota, Zang & Hall (1987) obtain weakly nonlinear solutions for TS waves, Dean vortices and mixed modes for $\eta \approx 2.179\times10^{-5}$. For $\eta \to 1$, Bennett & Hall (1986) examine the linear stability of nonlinear axisymmetric Dean vortices to TS waves.

For $\eta \approx (1-2.179\times10^{-5})$ the critical Reynolds numbers for axisymmetric and two-dimensional TS modes are close. Transition from plane Poiseuille flow can occur via a subcritical bifurcation so, depending on initial conditions, either type of instability could develop. The two modes may interact, yielding flows different from those induced by either mode alone (cf. Singer, Ferziger & Reed 1987).

For channels with aspect ratio $\Gamma \leqslant 5$, the two-dimensional numerical computations of Winters (1987), Shanthini & Nandakumar (1986), Schilling & Simon (1979), Cheng, Lin & Ou (1976) and Cheng & Akiyama (1970) describe axisymmetric curved channel flow with one or two pairs of vortices. Experiments and analytical approximations for square or nearly square channels, all for either axisymmetric or time-independent Dean vortices, are discussed in Berger, Talbot & Yao (1983); analogous results for Taylor–Couette flow suggest that most of these results are inapplicable to the large-aspect-ratio case. As well, we find the assumptions of axisymmetry and time independence to be valid only for a range of $Re > Re_c$, because Dean vortex flow bifurcates to a non-axisymmetric (wavy), time-periodic flow at higher Re. To our knowledge, the preliminary experiment of Kelleher, Flentie & McKee (1980), based on the theses by McKee (1973) and Flentie (1975), represents the extent of published experimental work on large-aspect-ratio curved channel flow. In a channel with $\Gamma = 40$, they measured the spanwise spacing of Dean vortices and presented flow visualizations. Except for very weakly curved channels, results on time-dependent Dean vortices are absent from the published literature. However, unpublished experiments by Niver (1987) suggest the presence of wavy vortices in curved channel flow.

Some work has been done on Dean vortices in turbulent curved channel flow. Experimentally, Hunt & Joubert (1979) observed turbulent Dean vortices with $Re \approx 125Re_c$. Using periodic spanwise boundary conditions in a curved channel with $\eta = 0.975$ and $Re \approx 20Re_c$, Moser & Moin (1984, 1987) performed a direct numerical simulation of turbulence. They observed turbulent Dean vortices and turbulence and discussed the interaction.

The large amount of work done on Taylor–Couette flow has revealed its rich nature (cf. DiPrima & Swinney 1985); similar work is needed on curved channel flow. Comparison with the plane channel is not useful, because plane channel flow undergoes a subcritical breakdown to turbulence (Nayfeh 1987), without the sequence of supercritical bifurcations found in curved channel flow. Görtler vortices in the concave boundary layer share some properties with Dean and Taylor vortices, e.g. they develop streamwise waviness, but in the boundary layer Re increases downstream resulting in a breakdown to turbulence without intermediate deterministic states (Bippes 1978).

We shall examine instability and transition in curved channel flow. Spanwise periodicity is imposed. The validity of this assumption is demonstrated by the results it produces in the Taylor–Couette problem; however, it fails to reproduce finite-span features (cf. Stuart 1986) which may occur in the curved channel. In addition, all curved channel flows that we present are fully developed. Channels with only short curved sections may not reach these fully developed states. We use $\eta = 0.975$, except

in §5, where $\eta = 0.875$ is also considered. For $\eta = 0.975$, $Re_c = 114.26$ and $a_c = 1.98$ (cf. §4).

In §2 we describe the code we use to find solutions of the Navier–Stokes equations. In §3 we discuss axisymmetric solutions containing Dean vortices, i.e. Dean vortex flow. In §4 we present linear and weakly nonlinear axisymmetric stability analyses; these predict some properties of Dean vortices. Sections 5–8 deal with two types of non-axisymmetric (wavy) Dean vortices: undulating and twisting Dean vortex flow. We examine the linear stability of Dean vortices to wavy disturbances in §5. Flow features of wavy vortices are given in §6. Approximate estimates of streamwise lengths required to reach these fully developed states are given in §7. In §8 we discuss possible wavy instability mechanisms. Concluding remarks are given in §9. Chaotic or non-deterministic behaviour does not occur for the range of parameters covered in this work.

2. Code implementation

Using the numerical method of Moser, Moin & Leonard (1983), we obtain three-dimensional time-dependent solutions of the incompressible Navier–Stokes equations for a curved channel. Periodic boundary conditions are used in the spanwise and streamwise directions. A pseudospectral method based on expansion functions that satisfy the continuity equation and the boundary conditions is used. Time-advancement is implicit for viscous terms and explicit for nonlinear (convective) terms. The code is a modification of the one used to study wavy Taylor vortices by Moser *et al.* (1983) and to perform a direct simulation of turbulence in the curved channel (Moser & Moin 1984, 1987). For later purposes, we define the discrete Fourier transform (in θ and z) of the velocity as $\hat{\boldsymbol{v}}$:

$$\boldsymbol{v}(\boldsymbol{x}, t) = \sum_{l=-L}^{L} \sum_{m=-M}^{M} \hat{\boldsymbol{v}}(r, k_\theta, k_z, t) \exp(\mathrm{i} k_\theta \theta) \exp(\mathrm{i} k_z z), \tag{2.1}$$

where

$$k_\theta = \frac{2\pi l}{L_\theta}, \quad -L \leqslant l \leqslant L; \qquad k_z = \frac{2\pi m}{L_z}, \quad -M \leqslant m \leqslant M \tag{2.2}$$

are wavenumbers; L_θ, L_z are the periods in θ and z; and $2L+1$ and $2M+1$ are the number of Fourier modes used. In practice, only the $(L+1)$ θ-modes with $0 \leqslant l \leqslant L$ are used, since a real-valued velocity implies:

$$\hat{\boldsymbol{v}}^*(r, k_\theta, k_z, t) = \hat{\boldsymbol{v}}(r, -k_\theta, -k_z, t), \tag{2.3}$$

where an asterisk indicates the complex conjugate. The spanwise computational domain initially includes one complete vortex, pair, i.e. $L_z = \lambda$. Because of the higher cost, we do not use random initial disturbances; instead, we use either a numerical solution at nearby (Re, a, η) or the lowest-order terms of an analytical solution due to Reid (1958) (cf. Finlay, Keller & Ferziger 1987*a*) that is appropriate to the narrow gap for Re and a on the linear neutral stability curve $Re_{ns}(a)$. The energies in the highest modes are monitored to ensure that adequate resolution is achieved. To eliminate aliasing errors, the nonlinear terms are evaluated in real space on a grid with $\frac{3}{2}$ as many grid points in each direction as the number of modes used in transform space.

3. Simulation of axisymmetric vortices

We now present steady axisymmetric solutions of the Navier–Stokes equations for $Re > Re_c$. These solutions contain Dean vortices but are not necessarily stable with respect to non-axisymmetric perturbations, as we shall see in §5.

All results in this section have $\eta = 0.975$; a less complete set of results for $\eta = 0.875$ indicates no important differences. We choose this η to compare with the experiment of Kelleher *et al.* (1980). We use a spanwise resolution of 19 or 29 Fourier modes, the higher resolution being used when the lower resolution yields a high-wavenumber upturn ('tail') in the spanwise energy spectrum. In the radial direction, we include Chebyshev polynomials through order 32.

In the cross-flow plane, contour plots of the cross-flow stream function and the streamwise perturbation velocity for one pair of Dean vortices are shown in figures 2 and 3 for $Re = 1.230Re_c$ and $a = 2.5$. The Stokes stream function in the (r, z)-plane is shown in figure 2. Each contour line is a projection of a streamline into this plane. We call $z = \frac{1}{2}\lambda$ the inflow plane, since the flow in this (r, θ)-plane is towards the inner wall; we term $z = \lambda$ the outflow plane. The streamwise flow is perpendicular to and out of the plane of the plot. The inflow region has larger radial velocities than the outflow region. This is opposite to the behaviour of Taylor vortices in the usual configuration with the inner cylinder rotating (cf. Jones 1985; Marcus 1984).

The contour plot of the streamwise perturbation velocity u_θ is shown in figure 3, where $u_\theta(r, z) \equiv v_\theta(r, z) - V(r)$, v_θ is the total streamwise velocity, and V is the CCPF velocity profile:

$$\left.\begin{aligned} V(r) &= A\left(r \ln r + Cr + \frac{E}{r}\right), \\ \text{where} \qquad C &= \frac{r_i^2 \ln r_i - r_o^2 \ln r_o}{r_o^2 - r_i^2}, \quad E = -\frac{r_i^2 r_o^2}{r_o^2 - r_i^2} \ln \eta, \quad A = -\frac{2}{r_c + E \ln \eta}. \end{aligned}\right\} \tag{3.1}$$

Except for CCPF,

$$V(r) \neq \int_0^\lambda v_\theta(r, z)\, dz/\lambda.$$

All velocities are normalized with respect to the mean streamwise velocity $\bar{U}$. The general features of figure 3 can be explained by examining the secondary flow streamlines shown in figure 2. For example, the inflow near $z = \frac{1}{2}\lambda$, $r = r_o$ draws fluid with low streamwise velocity from the outer wall to the middle of the channel. This produces a negative streamwise perturbation velocity near $z = \frac{1}{2}\lambda$, $r = r_o - \frac{1}{4}d$. The normal and spanwise velocities, u_z and u_r, have amplitudes an order of magnitude smaller than the streamwise perturbation velocity (cf. Finlay, Keller & Ferziger 1987*a*, *b*).

If $z = 0$ is either an inflow or an outflow plane, the flow has reflection symmetry about it:

$$\left.\begin{aligned} u_\theta(r, z) &= u_\theta(r, \lambda - z), \\ u_r(r, z) &= u_r(r, \lambda - z), \\ u_z(r, z) &= -u_z(r, \lambda - z). \end{aligned}\right\} \tag{3.2}$$

This is the axisymmetric version of shift-and-reflect symmetry (Marcus 1984). Although we do not enforce the relations between Fourier modes that (3.2) infers, they were obeyed to within roundoff error.

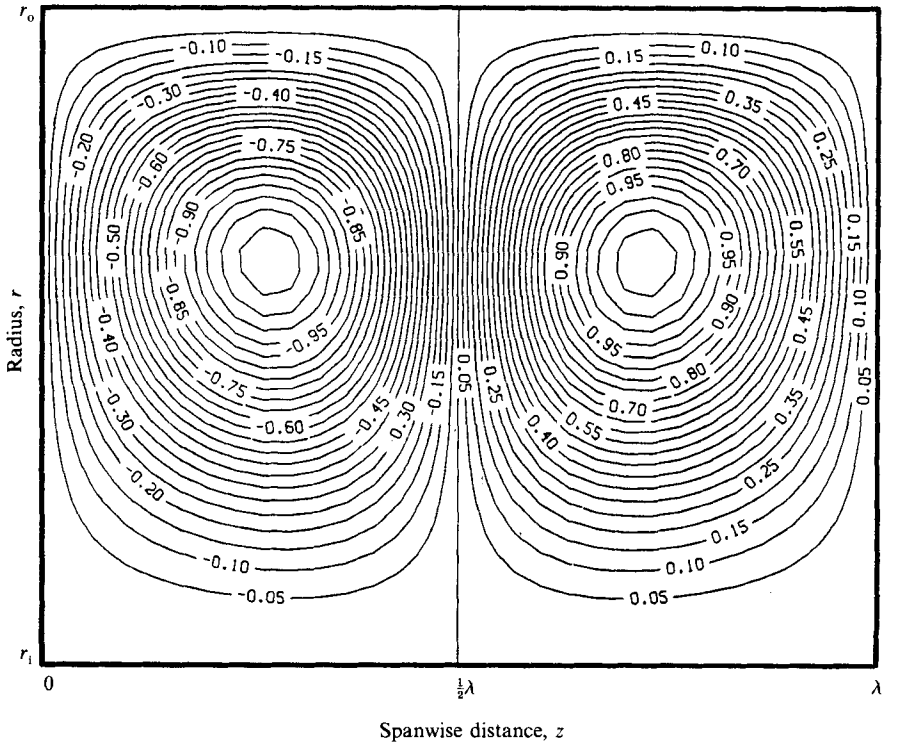

FIGURE 2. Contours of Stokes stream function in an (r, z)-plane at $Re = 1.230Re_c$, $a = 2.5$.

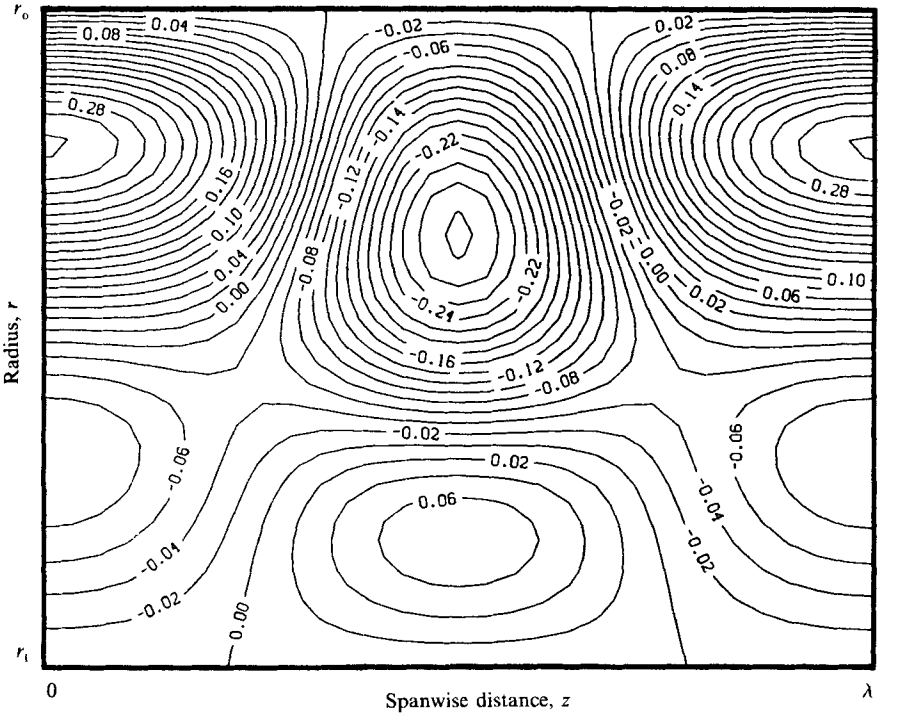

FIGURE 3. Contours in an (r, z)-plane of streamwise perturbation velocity u_θ, at $Re = 1.230Re_c$, $a = 2.5$.

A measure of the strength of the vortices is the pressure-gradient parameter Δp, defined as

$$\Delta p \equiv \frac{\overline{\frac{\partial p}{\partial \theta}} - \frac{\partial P}{\partial \theta}}{\overline{\frac{\partial P}{\partial \theta}}}, \tag{3.3}$$

where $-(1/r)(\partial p/\partial\theta)$ is the streamwise pressure gradient, $\overline{\partial p/\partial\theta}$ is the value of $\partial p/\partial\theta$ averaged over the computational box, and $-(1/r)(\partial P/\partial\theta)$ is the streamwise pressure gradient for CCPF. We compute only the velocity, but $\overline{\partial p/\partial\theta}$ can be obtained from the mean shear stress at the walls:

$$\overline{\frac{\partial p}{\partial \theta}} = -\frac{1}{2Re}\left(r_i \frac{\partial V_\theta}{\partial r}\bigg|_{r_i} - r_o \frac{\partial V_\theta}{\partial r}\bigg|_{r_o}\right), \tag{3.4}$$

where $V_\theta(r)$ is the spanwise–streamwise average of the total streamwise velocity, v_θ. It can be shown analytically for axisymmetric flow (cf. §4) that $\partial p/\partial\theta$ is independent of r, z and θ. From the θ-momentum equation for CCPF we find

$$\frac{\partial P}{\partial \theta} = -4/\left\{Re\left[r_c - \frac{(r_c^2-1)^2}{4r_c}(\ln\eta)^2\right]\right\}. \tag{3.5}$$

All pressures are non-dimensionalized by $\rho\bar{U}^2$.

The quantity Δp plays a role similar to that of the Nusselt number in Rayleigh–Bénard convection, or the non-dimensional torque in Taylor–Couette flow. Values of Δp for various Re and a are shown in figure 4. The points with $\Delta p = 0$ are obtained from linear stability analysis. Because u_θ is larger than u_r and u_z, the circulation around a vortex and the mass flow across a plane between two vortex centres are not necessarily good measures of the vortex strength. In §4, we shall show that for Re close to the neutrally stable value, Re_{ns}, Δp is linear in $(Re - Re_{ns})$.

Variations of vortex shape with changing a, Re are discussed in Finlay *et al.* (1987*a*, *b*).

3.1. *Energy spectra*

The energy in z-Fourier modes decreases exponentially with increasing $|k_z|$, where $k_z = 2\pi m/a$. For steady axisymmetric flows we define the energy in spanwise modes $\pm k_z$ as

$$E(k_z) = c(k_z)\int_{r_i}^{r_o} |\hat{v}(r, k_z)|^2 \, dr. \tag{3.6}$$

Here, $\hat{v}(r, k_z)$ is the Fourier transform with respect to z of the velocity (see (2.1)), and

$$c(k) = \begin{cases} \frac{1}{2} & k = 0, \\ 1 & k \neq 0. \end{cases} \tag{3.7}$$

Equation (3.6) accounts for the energy in both modes $\pm k_z$, so the kinetic energy ($\frac{1}{2}v^2$) of the flow is given by $\sum_{m=0}^{M} E(k_z)$.

We find $\ln E(k_z)$ is linear in $|k_z|$ except for $|k_z|$ near zero. A plot of $\ln E(k_z)$ versus k_z is shown in figure 5 for $Re = 1.230 Re_c$ and several a. Similar behaviour was observed by Marcus (1984) for Taylor vortices. The explanation of Marcus (1984) can be adapted to Dean vortices as follows.

The mean pressure gradient supplies energy only to the $k_z = 0$ mode; for $k_z \neq 0$ the only source of energy is nonlinear interactions among triads of modes $\pm k_z$, k_z',

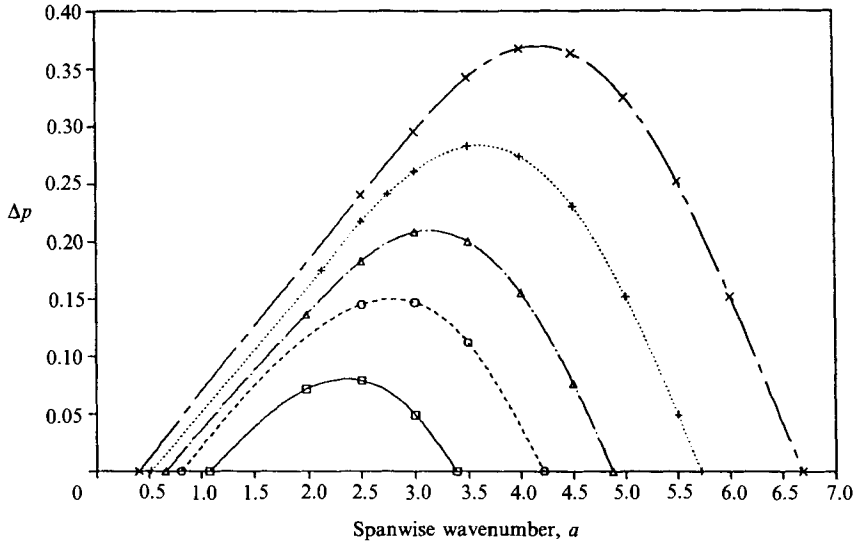

FIGURE 4. Δp for axisymmetric vortices as a function of Re and a: □, $Re = 1.230Re_c$; ○, $1.503Re_c$; △, $1.776Re_c$; +, $2.186Re_c$; ×, $2.733Re_c$. The lines are included to guide the eye.

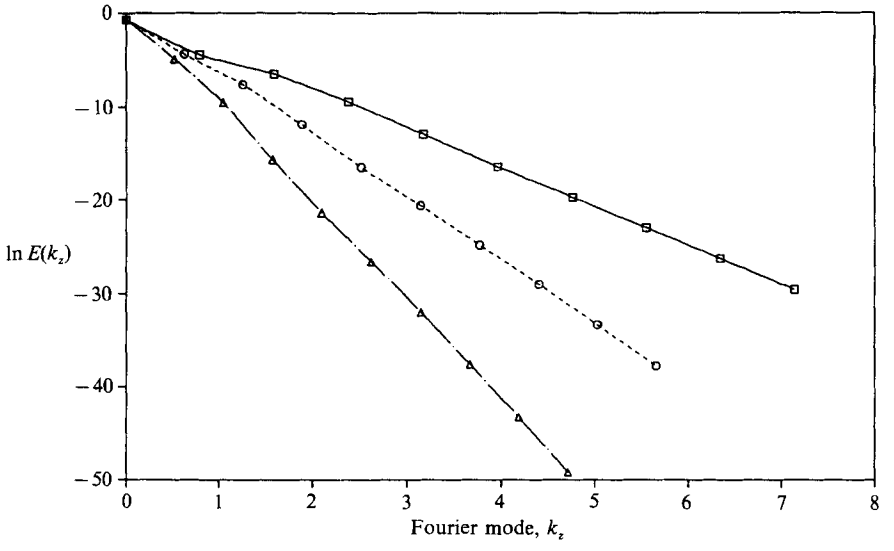

FIGURE 5. The kinetic energy in the spanwise Fourier modes $|k_z|$ as a function of $|k_z|$ for several a at $Re = 1.230Re_c$; □ (——), $a = 1.98$; ○ (– – –), 2.5; △ (—·—), 3.

$\mp k_z - k_z'$. Most of the energy coming into k_z is viscously dissipated and only smaller wavenumber modes, k_z', supply energy to k_z. For sufficiently large k_z these are reasonable assumptions. With the additional assumption that ln E obeys a power law:

$$\ln E(k_z) = -\gamma |k_z|^\beta + \text{constant}, \tag{3.8}$$

it can be shown that $\beta = 1$.

The slope $-\gamma$ decreases with increasing a, as shown in figure 5. The quantity $1/|\gamma|$ is a measure of the fraction of energy passed on to higher wavenumbers from each k_z. Larger a indicates more closely spaced vortices; therefore, with increasing a,

we might expect less energy to be transferred from k_z, because the shorter spanwise lengthscale causes more dissipation to occur within k_z.

3.2. *Vortex doubling*

With Re fixed, we find that a bifurcation to two pairs of vortices can occur as a is decreased. An additional pair of vortices appears in the steady-state solution and increases continuously in strength and size as a is decreased over a small range (cf. Finlay *et al.* 1987*a*). Continuation methods (Keller 1977) should yield results similar to those observed for bifurcations from two to four vortices in spanwise periodic Taylor–Couette flow (e.g. Meyer-Spasche & Keller 1985).

With increasing Re similar bifurcations occur. At $a = 1.98$, a small pair of secondary vortices appears for Re between $1.776Re_c$ and $2.186Re_c$, centred on the inflow plane next to the convex wall (cf. Finlay *et al.* 1987*a*). The secondary pair grows in size and strength as Re increases. For $\eta = 0.979$, $\Gamma = 40$ and $Re > 2Re_c$, similar secondary vortices were found experimentally by P. Ligrani (1987, private communication). Using continuation methods, Winters (1987) describes a complex bifurcation set in the parameters $(\eta, \Gamma, \Delta p)$ for transitions between one and two pairs of axisymmetric vortices in curved channels with $\Gamma \leqslant 1.5$. Shanthini & Nandakumar (1986), Cheng *et al.* (1976), Joseph, Smith & Adler (1975) and Cheng & Akiyama (1970) performed axisymmetric computations in finite-span curved channels with aspect ratio $\Gamma \leqslant 5$ and found secondary vortices appearing with increasing Re. Hunt & Joubert (1979) observed turbulent Dean vortices with pairs of weaker secondary vortices occurring between the stronger primary pairs in a curved-channel experiment with $Re \approx 125Re_c$, $a \approx 2.17$, $\eta = 0.99$, $\Gamma = 13.2$.

In Taylor–Couette flow for given Re and η, linear neutral stability analysis predicts that a band of Taylor vortex wavenumbers a can occur. For a outside this range the flow decays to laminar azimuthal flow. It has been found, however, that the band of stable wavenumbers is made smaller by an Eckhaus instability (Dominguez-Lerma, Cannell & Ahlers 1986; Riecke & Paap 1986; Kogelman & Diprima 1970), in which Taylor vortices are unstable to axisymmetric disturbances. Experimentally, when the Eckhaus stability boundary is crossed, the number of vortices in the finite-length system usually changes by two (Ahlers, Cannell & Dominguez-Lerma 1983); that is, a pair is gained or lost. In his numerical simulations of wavy Taylor vortices using periodic spanwise boundary conditions, Marcus (1984) observed a vortex-doubling bifurcation (by decreasing a at fixed Re and η) close to the Eckhaus stability boundary found experimentally by King & Swinney (1983) for wavy Taylor vortices. We have not examined the Eckhaus stability of Dean vortices, but the presence of a vortex-doubling bifurcation may indicate an Eckhaus instability in the curved channel. The lower a limit of the Eckhaus stability band may be near the vortex-doubling bifurcation we observe (cf. Finlay *et al.* 1987*a*).

4. Semi-analytical treatment of axisymmetric vortices

In this section we present semi-analytical methods for predicting the properties and stability of axisymmetric vortices by treating them as a perturbation of CCPF. The simplest analytical approach assumes an inviscid fluid. If we define

$$\Phi \equiv \frac{1}{r^3}\frac{\mathrm{d}}{\mathrm{d}r}[(rV)^2], \tag{4.1}$$

where V is the streamwise velocity of the fluid, then for a flow with concentric circular streamlines, a necessary and sufficient condition for inviscid stability to axisymmetric perturbations is $\Phi(r) \geqslant 0$ everywhere in the flow field (Rayleigh 1916). For the curved channel, using the CCPF velocity profile (3.1) for $V(r)$, we find that $\Phi < 0$ when $r > r_\Phi \equiv e^{-\frac{1}{2}} e^{-C}$, and C is given in (3.1). The value of r_Φ increases from r_c for $\eta \sim 1$, to $r_\Phi = r_c + 0.057d/2$ at $\eta = 0.5$; thus the flow is always inviscidly unstable. Inviscid stability theory cannot predict a critical value of the Reynolds number, Re_c. Previous authors (see §1) found Re_c using linear neutral stability analysis. We now turn to linear and weakly nonlinear analysis with $Re > Re_c$.

Using the framework of weakly nonlinear theory, it is expedient to derive simultaneously the linear and weakly nonlinear equations for Dean vortices. Linear stability analysis yields temporal growth rates for small-amplitude axisymmetric disturbances to CCPF. Weakly nonlinear analysis provides values of Δp; we shall compare these values with those obtained from fully nonlinear simulation to provide insight into the validity of the weakly nonlinear analysis. The following analysis closely parallels the procedure given by DiPrima (1967) or Davey (1962) for the Taylor vortex problem (see also Stuart 1960; Watson 1960). The reader is referred there or to Finlay *et al.* (1987*a*) for a more complete exposition.

As discussed in §1, if we restrict our analysis to $\eta < (1 - 2.179 \times 10^{-5})$, we do not need to consider either two-dimensional Tollmien–Schlichting or mixed modes.

For given Re, a and η, the axisymmetric flow in a curved channel can be characterized as a perturbation to purely azimuthal flow:

$$v_r = u(r,z,t), \quad v_\theta = v(r,z,t) + V(r), \quad v_z = w(r,z,t), \quad p = p'(r,z,t,\theta) + P(r,\theta), \tag{4.2}$$

where the CCPF solution provides the velocity V and pressure P. Substituting (4.2) into the Navier–Stokes equations, we find that $\partial p'/\partial\theta$ is independent of r, z and θ, and $\partial P/\partial\theta$ is independent of r, z, θ, t. As a result, we define

$$\frac{\partial p'}{\partial \theta} = h_0(t) \tag{4.3}$$

and

$$\frac{\partial P}{\partial \theta} = H = \text{constant}. \tag{4.4}$$

Following Davey (1962) we expand the perturbation flow in Fourier series:

$$\left.\begin{aligned} v(r,z,t) &= v_0(r,t) + \sum_{n=1}^{\infty} v_n(r,t) \cos naz, \\ p'(r,z,t,\theta) &= p_0(r,t,\theta) + \sum_{n=1}^{\infty} p_n(r,t) \cos naz, \\ u(r,z,t) &= \sum_{n=1}^{\infty} nau_n(r,t) \cos naz, \\ w(r,z,t) &= \sum_{n=1}^{\infty} w_n(r,t) \sin naz, \end{aligned}\right\} \tag{4.5}$$

and also in power series of an as yet unknown amplitude A:

$$v_0(r,t) = A^2(t)\left[v_{00}(r) + \sum_{m=1}^{\infty} A^{2m}(t)\, v_{0m}(r)\right], \tag{4.6}$$

$$\boldsymbol{Q}_n(r,t) = A^n(t)\left[\boldsymbol{Q}_{n0}(r) + \sum_{m=1}^{\infty} A^{2m}(t)\, \boldsymbol{Q}_{nm}(r)\right], \tag{4.7}$$

$$h_0 = A^2(t)\left[h_{00} + \sum_{m=1}^{\infty} A^{2m}(t)\, h_{0m}\right], \tag{4.8}$$

$$\frac{\mathrm{d}A}{\mathrm{d}t} = \sigma A + a_1 A^3 + a_2 A^5 + \ldots, \tag{4.9}$$

where $\boldsymbol{Q}_n = (u_n, v_n)$ and $\boldsymbol{Q}_{nm} = (u_{nm}, v_{nm})$.

The appearance of the linear growth rate σ in (4.9) is consistent with the $O(A)$ exponential temporal growth prediction of linear stability analysis. Here, σ is assumed to be real, which is the 'exchange of stabilities' ansatz and indicates a Landau type of bifurcation (Drazin & Reid 1981). That σ is real and not complex is verified by the exponential growth we observe in nonlinear runs with weak axisymmetric vortices. We now substitute (4.2)–(4.9) into the Navier–Stokes equations with appropriate boundary conditions. Terms $O(A)$ give the linear stability problem, that is

$$(\mathbf{L}_1 + \sigma \mathbf{M}_1)\, \boldsymbol{Q}_{10} = 0, \quad u_{10} = \mathrm{D}u_{10} = v_{10} = 0 \quad \text{at } r = r_\mathrm{i}, r_\mathrm{o}, \tag{4.10}$$

where $\mathbf{L}_1$ and $\mathbf{M}_1$ are matrix differential operators given in the Appendix. We solved (4.10) numerically using an initial-value method.

For $\sigma = 0$ and given η, this eigenvalue problem yields the neutral stability curve $Re_{\mathrm{ns}}(a)$, found by previous authors. For fixed $\sigma > 0$ and given η, curves through the values of Re and a with equal linear growth rates are obtained. From these curves, it is apparent that, for each Re, there is a wavenumber that has maximum growth rate. Figure 6 gives the curve joining the values of a having maximum σ at each Re. Also shown is the curve joining the a values having maximum Δp at various Re, obtained from figure 4. The finite-amplitude Dean vortices observed experimentally by Kelleher *et al.* (1980) had wavenumber $a \approx 2.55$ for all three Reynolds numbers $2.14Re_\mathrm{c} \leqslant Re \leqslant 3.07Re_\mathrm{c}$ they examined; a varied across the span of their channel. This variation is indicated in figure 6 by adding standard-deviation error bars to the three data points presented by Kelleher *et al.* (1980). (Their channel had $\Gamma = 40$ and $\eta = 0.979$ and their vortices were probably non-axisymmetric (cf. §7).) The turbulent Dean vortices in the experiment of Hunt & Joubert (1979) had $a \approx 2.17$ for $Re \approx 125Re_\mathrm{c}$, $\eta = 0.99$ and a channel with aspect ratio $\Gamma = 13.2$. Based on figure 6, maximizing σ or Δp does not select a. Above Re_c, linear stability analysis predicts a band of stable wavenumbers. This band is probably narrowed by an Eckhaus stability boundary (cf. §3.2). Any a in this Eckhaus stable band may occur, and non-uniformities in the initial flow and channel walls probably affect the wavenumber selection. Based on results obtained for Taylor–Couette flow, this band might be further restricted by adding a spanwise section of channel in which the channel width varies (cf. Dominguez-Lerma *et al.* 1986).

Returning to the weakly nonlinear analysis, we do not expand the linear growth rate as

$$\sigma = \sigma_0 \epsilon + O(\epsilon^2), \tag{4.11}$$

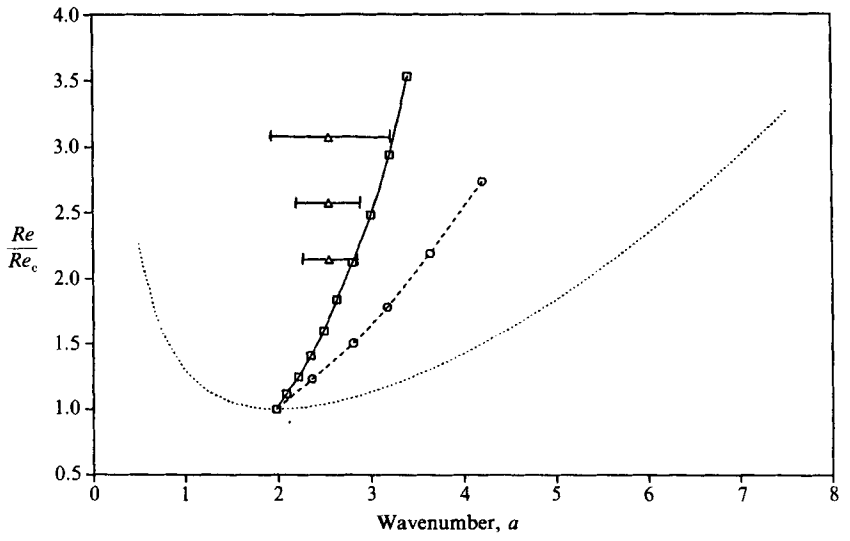

FIGURE 6. Curves of maximum linear growth rate (□, ——), maximum Δp (○, – – – –); and the data of Kelleher *et al.* (1980) (△) with error bars included by us. The axisymmetric neutral stability curve $Re_{ns}(a)$ (·····) is included for reference.

where $\epsilon = Re - Re_{ns}$, as some authors have done for the Taylor vortex problem (Davey 1962; also see DiPrima & Swinney 1985). Instead, we use the σ calculated from linear stability analysis. If σ is assumed to depend on Re according to (4.11), we shall find that $A = O(\epsilon^{\frac{1}{2}})$ for small ϵ. From (4.7), this implies that the amplitude of the nth Fourier mode behaves asymptotically as $\boldsymbol{Q}_n = O(\epsilon^{n/2})$. In the Taylor vortex problem this asymptotic behaviour holds up to the surprisingly large value of $\epsilon/Re_c \approx 1$ at a_c and $\eta = 0.612$ (Gollub & Freilich 1976); however, this does not occur in our nonlinear simulations. For example, at the critical wavenumber and $\eta = 0.975$, the fundamental Fourier mode $\boldsymbol{Q}_1$ approximately obeys the asymptotic power law only for $\epsilon/Re_c < 0.1$.

Terms $O(A^2)$ in the substitution of (4.2)–(4.9) into the Navier–Stokes equations give

$$\left(-\frac{\mathrm{DD}^*}{Re} + 2\sigma\right) v_{00} = -\frac{a}{2}\left(\mathrm{D}^* + \frac{1}{r}\right) u_{10} v_{10} - \frac{h_{00}}{r}, \tag{4.12}$$

$$v_{00} = 0 \quad \text{at } r = r_i, r_o, \tag{4.13}$$

and

$$(\mathbf{L}_2 + 2\sigma \mathbf{M}_2)\, \boldsymbol{Q}_{20} = \boldsymbol{S}_{20}, \tag{4.14}$$

$$u_{20} = \mathrm{D}u_{20} = v_{20} = 0 \quad \text{at } r = r_i, r_o. \tag{4.15}$$

Here D, D* are differential operators given in (A 5); $\boldsymbol{S}_{20}$ is a quadratic function of the linear stability eigenfunctions u_{10}, v_{10}, and $\mathbf{L}_2$ and $\mathbf{M}_2$ are matrix differential operators. These are given in the Appendix.

With (4.10) solved, $\boldsymbol{S}_{20}$ is determined and $\boldsymbol{Q}_{20}$ can be found. We solve (4.14) and (4.15) using an initial-value method similar to that used in solving (4.10). We solve (4.12) and (4.13) using a shooting method. The constant h_{00} is determined by solving (4.12) and (4.13) subject to the mass flux constraint

$$\int_{r_i}^{r_o} v_{00}\, \mathrm{d}r = 0, \tag{4.16}$$

which follows from $O(A^2)$ terms in

$$\int_{r_i}^{r_o}\int_0^{\lambda} v_\theta \,\mathrm{d}z\,\mathrm{d}r = \bar{U}. \tag{4.17}$$

Recall that one objective of this analysis is to find the pressure-gradient parameter Δp. From (3.3), (4.3), (4.4) and (4.8) we have, to $O(A^2)$:

$$\Delta p = \frac{h_{00}A^2}{H}. \tag{4.18}$$

The value of H from (4.4) is given in (3.5).

From our fully nonlinear simulations we know that a steady solution is reached, so that the Landau constant a_1 in (4.9) is negative (the instability is supercritical). The steady-state value of A is determined from (4.9) by neglecting terms $O(A^5)$ and letting $t\to\infty$, which gives

$$A = \left(\frac{\sigma}{-a_1}\right)^{\frac{1}{2}}. \tag{4.19}$$

Substituting this equation into (4.18), we have

$$\Delta p = \left(\frac{h_{00}}{H}\right)\frac{\sigma}{-a_1}. \tag{4.20}$$

The only unknown remaining on the right-hand side of (4.20) is the Landau constant a_1. We determine a_1 in the manner outlined in DiPrima (1967); the reader is referred there or to Finlay *et al.* (1987*a*) for the derivation of the following formula:

$$a_1 = \frac{(\boldsymbol{S}_{13}\,|\,\boldsymbol{Q}_{10}^+)}{(\mathbf{M}_1\boldsymbol{Q}_{10}\,|\,\boldsymbol{Q}_{10}^+)}. \tag{4.21}$$

The notation $(\boldsymbol{f}\,|\,\boldsymbol{g})$ indicates the inner product

$$(\boldsymbol{f}\,|\,\boldsymbol{g}) = \int_{r_i}^{r_o}\sum_{i=1}^{2} r f_i g_i \,\mathrm{d}r, \quad \text{where } \boldsymbol{f} = (f_1, f_2),\ \boldsymbol{g} = (g_1, g_2). \tag{4.22}$$

In (4.21), $\boldsymbol{S}_{13}$ is a function of $u_{10}, u_{20}, v_{00}, v_{10}, v_{20}$ given in the Appendix; it appears in the equation obtained by keeping terms $O(A^3)$ with $n = 1$ in (A 8):

$$\left.\begin{aligned}(\mathbf{L}_1 + 3\sigma\mathbf{M}_1)\,\boldsymbol{Q}_{11} &= -a_1\,\mathbf{M}_1\boldsymbol{Q}_{10} + \boldsymbol{S}_{13},\\ u_{11} = \mathrm{D}u_{11} &= v_{11} = 0 \quad \text{at } r = r_i, r_o.\end{aligned}\right\} \tag{4.23}$$

In (4.21), $\boldsymbol{Q}_{10}^+$ is the solution of the equation adjoint to (4.10), i.e.

$$(\mathbf{L}_1^{\mathrm{t}} + \sigma\mathbf{M}_1^{\mathrm{t}})\,\boldsymbol{Q}_{10}^+ = 0, \quad u_{10}^+ = \mathrm{D}u_{10}^+ = v_{10}^+ = 0 \quad \text{at } r = r_i, r_o, \tag{4.24}$$

where superscript t indicates matrix transpose. Equation (4.24) is solved in the same manner as (4.10).

Equations (4.10), (4.12)–(4.15) and (4.24) must be solved to obtain a_1 from (4.21) and, finally, to evaluate Δp from (4.20). Comparisons of the values of Δp obtained in this manner to those obtained by the fully nonlinear simulations presented earlier are shown for various a and Re in figure 7. For Re near Re_{ns}, it can be seen from (4.11), (4.20) that Δp behaves linearly with $(Re - Re_{\mathrm{ns}})$. At large a the weakly nonlinear approximation gives excellent results well into the nonlinear region, as shown in figure 7(*b*, *c*). For smaller a, however, nonlinearities involving modes neglected by

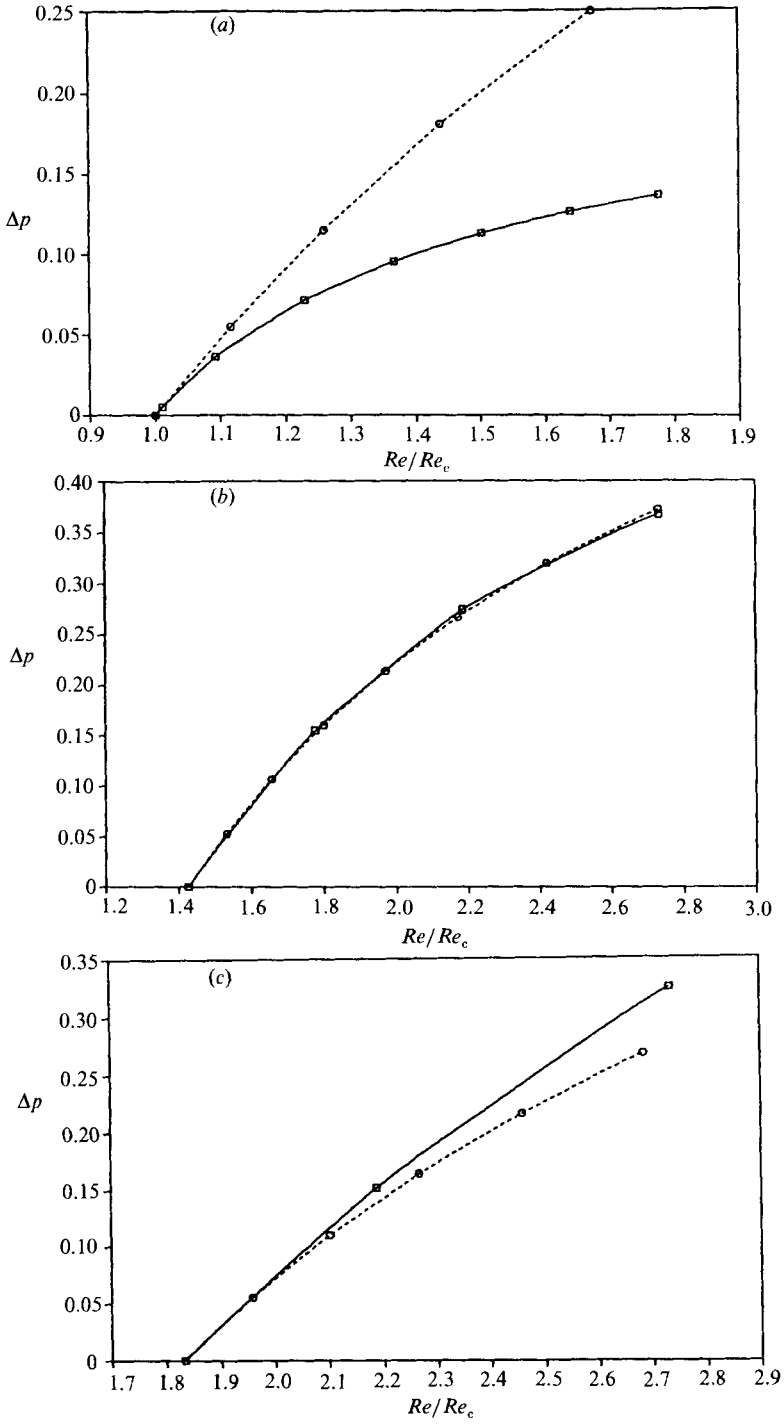

FIGURE 7. Comparison of pressure-gradient parameter Δp obtained from weakly nonlinear theory (○, ----), and full nonlinear simulation (□, ——), for various Re, and (*a*), $a = 1.98$, (*b*) $a = 4$; (*c*) $a = 5$.

the weakly nonlinear approximation are important, and the accuracy of the weakly nonlinear approximation is seriously impaired at higher Re, as shown in figure 7(*a*). These observations are consistent with the result discussed in §3.1 that the slope, $-\gamma$, of energy spectra (see (3.8)) becomes steeper with increasing a. The value of $E(6\pi/a)/E(2\pi/a)$ is the ratio of the energy in the most energetic mode neglected by the weakly nonlinear theory to the energy in the fundamental mode. From full simulations, we find $E(6\pi/a)/E(2\pi/a)$ to be approximately 35 times larger at $a = 2.5$ than at $a = 5.0$ for the same value of $\epsilon = Re - Re_{\rm ns} \approx 30$. The accuracy of the $O(A^2)$ weakly nonlinear assumption clearly depends on a as well as Re.

5. Linear stability of Dean vortex flow to non-axisymmetric perturbations

We now examine the linear stability of Dean vortices to non-axisymmetric (wavy) disturbances by writing the flow as

$$\boldsymbol{v}(r,\theta,z,t) = \boldsymbol{u}(r,z)\,\mathrm{e}^{(\sigma-\mathrm{i}\omega)t}\,\mathrm{e}^{\mathrm{i}\beta\theta} + \boldsymbol{v}^{\rm D}(r,z), \tag{5.1}$$

where $\boldsymbol{v}^{\rm D}(r,z)$ represents an axisymmetric vortex flow obtained as in §3. The physical velocity field is the real part of (5.1). The complex temporal growth rate, $\sigma - \mathrm{i}\omega$, allows oscillatory growth or decay. The parameter β is a given real-valued streamwise wavenumber. The streamwise wavelength is

$$\mu = 2\pi/\beta.$$

The curved channel geometry defined in §1 must have continuous streamwise extent less than 2π rad. Channels that spiral inward (or outward) can have longer streamwise lengths, but they do not have constant curvature; therefore, they do not satisfy our curved channel definition. Based on these considerations, we restrict our attention to $\beta \geqslant 1$. Equation (5.1) implies that the non-axisymmetric disturbance travels with angular speed

$$\Omega = \omega/\beta. \tag{5.2}$$

For given (Re, a, η), we examine the stability of non-axisymmetric perturbations with given β by substituting (5.1) into the Navier–Stokes equations. We could linearize the resulting partial differential equations, but instead choose to use the three-dimensional nonlinear code described in §2. Disturbances with spanwise period different from that of $\boldsymbol{v}^{\rm D}$ are not considered; therefore, we cannot observe the subharmonic modes that occur in Taylor–Couette flow for $\eta < 0.5$ (Iooss 1986; Jones 1985). We choose the streamwise length of the computational region to be $2\pi/\beta$. The initial conditions contain a weak non-axisymmetric perturbation from $\boldsymbol{v}^{\rm D}$. The solution progresses in time until $\mathrm{e}^{(\sigma-\mathrm{i}\omega)t}$ time dependence occurs. We use 19 spanwise Fourier modes, 7 streamwise Fourier modes ($M = 9$ and $L = 3$ in (2.1)), and Chebyshev polynomials up to order 32 in the radial direction.

If $z = 0$ is at either an inflow or an outflow plane of Dean vortex flow, then a non-axisymmetric perturbation is called 'in phase' if it satisfies the same reflection symmetry property as the flow it is perturbing, i.e. if it satisfies (3.2). An out-of-phase mode satisfies (3.2) with λ replaced by $\frac{1}{2}\lambda$. In general, a non-axisymmetric perturbation is neither in phase nor out of phase, but is a linear combination of these two types of modes. For $\eta > 0.5$ and a stationary outer cylinder, Taylor vortices are linearly stable to in-phase non-axisymmetric disturbances (Davey, DiPrima & Stuart 1968; Jones 1981; Jones 1985). Instability is determined by disturbances that are out of phase; this is true for Dean vortices as well. Energy in in-phase modes decays rapidly, leaving significant energy only in the out-of-phase modes. For the

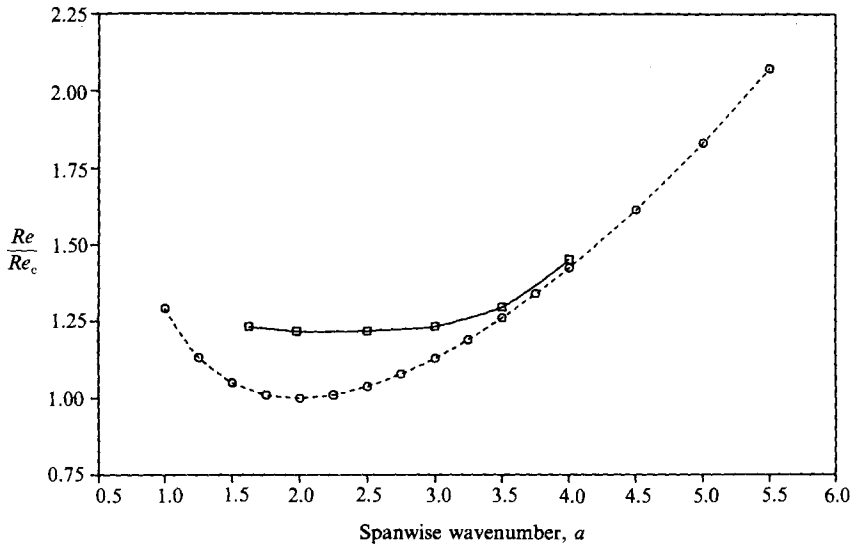

FIGURE 8. Neutral stability curve $Re'_{ns}(a)$ (□, ——) for non-axisymmetric disturbances to Dean vortex flow, at $\eta = 0.975$. Included for reference is the neutral stability curve $Re_{ns}(a)$ (○, – – –) for axisymmetric disturbances to CCPF.

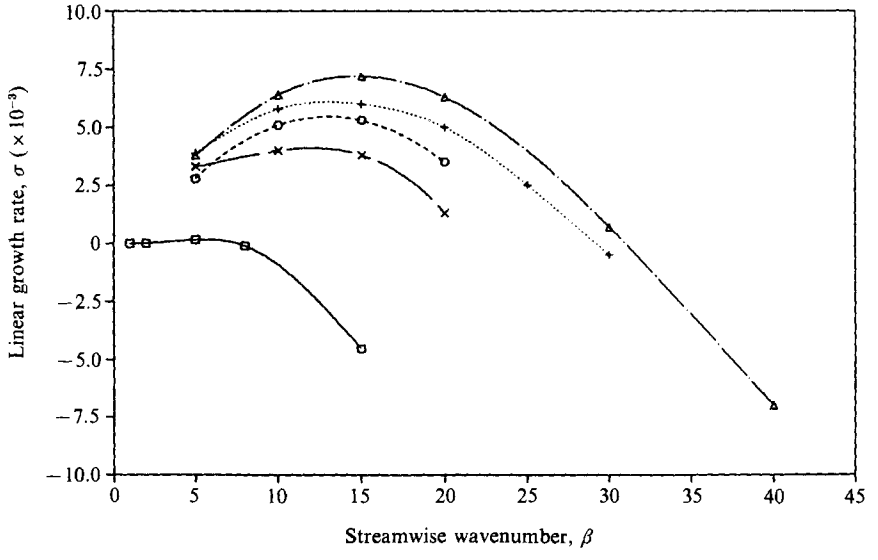

FIGURE 9. Linear growth rate, σ, of non-axisymmetric disturbances to Dean vortex flow (at $a = 2.5$, $\eta = 0.975$) as a function of $\beta \leqslant 40$, and Re: □, $Re = 1.230Re_c$; ○, $1.503Re_c$; △, $1.776Re_c$; +, $2.186Re_c$; ×, $2.733Re_c$.

Re, a, β, η we consider, all sufficiently small-amplitude growing disturbances of the form (5.1) are out of phase to within roundoff error. Fully developed, nonlinear, non-axisymmetric Dean vortices are neither in phase nor out of phase, which is also true for wavy Taylor vortices (Marcus 1984).

For given η, we obtain $\sigma - i\omega$ at various (Re, a, β) and determine a neutral stability curve $Re'_{ns}(a)$. For $\beta \geqslant 1$, we find that disturbances with $\beta = 1$ become unstable at the lowest Re. The neutral stability curve $Re'_{ns}(a)$ is shown in figure 8. The value of

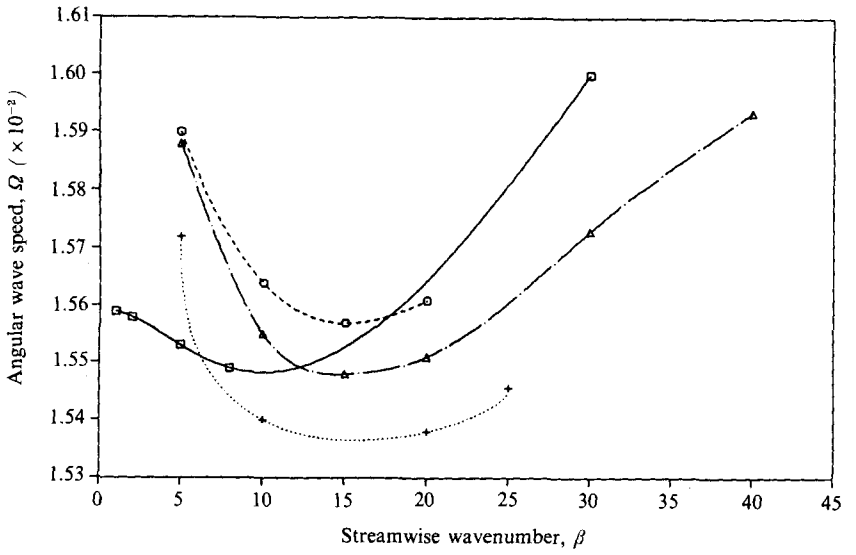

FIGURE 10. Angular wave speed Ω of small-amplitude non-axisymmetric disturbances to Dean vortex flow (at $a = 2.5$, $\eta = 0.975$) as a function of $\beta \leqslant 40$, and Re: □, $Re = 1.230Re_c$; ○, $1.503Re_c$; △, $1.776Re_c$; +, $2.186Re_c$.

$Re'_{ns}(a)$ is not given for $a < 1.6$ because an additional pair of axisymmetric vortices appears in $\boldsymbol{v}^D$ (cf. §3.2). The neutral stability curve $Re_{ns}(a)$ for perturbations of CCPF by axisymmetric disturbances is included for reference. From figure 8 it is seen that axisymmetric vortices are stable to non-axisymmetric disturbances only for a small range of Re above Re_c. This is also observed in Taylor–Couette flow at this radius ratio (Jones 1981).

Figure 9 gives $\sigma(\beta)$ for several Re at $a = 2.5$, $\eta = 0.975$. Although $\beta = 1$ is the first to become unstable, modes with $\beta > 1$ have larger positive growth rates for $Re > Re'_{ns}$. For $Re \geqslant 1.503Re_c$, the maximum growth rate occurs near $\beta \approx 15$.

As in Taylor–Couette flow, the angular speed, Ω, of the travelling wave is only weakly dependent on the parameters Re, a, β. For $a = 2.5$, $\Omega(\beta)$ is given at several Re in figure 10. These values are for small-amplitude disturbances; the nonlinear wave speeds are slightly different (cf. §6 and figure 21). For a in the range considered here, figures 9 and 10 do not change qualitatively with a. (See Finlay *et al.* 1987*a* for the variation of σ and Ω with a.)

Examining non-axisymmetric disturbances at higher β, we find behaviour not observed in Taylor–Couette flow. For fixed a, the disturbance with largest positive growth rate shifts to much higher β when Re increases above a certain value. For $a = 2.5$ and $\eta = 0.975$, this result is depicted in figure 11; a larger range of Re and β than in figure 9 is shown. There are two local maxima in $\sigma(\beta)$; we define β_u and β_t as the positions of the maxima with lower and higher β, respectively. Both β_t and β_u depend on Re, a, η. As shown in the following sections, wavy Dean vortex flows for the two ranges of β are dissimilar. We use the terms 'twisting' and 'undulating' vortices to mean wavy vortices with β near β_t and β_u, respectively. For the Re shown in figure 11, $\sigma(\beta_t)$ increases monotonically with increasing Re. In contrast, $\sigma(\beta_u)$ increases from zero, at Re'_{ns}, to a maximum at some Re and then decreases with further increases in Re; this is shown clearly in figure 9. We define Re''_{ns} as the value of Re at which $\sigma(\beta_t) = 0$. It represents the Reynolds number above which twisting

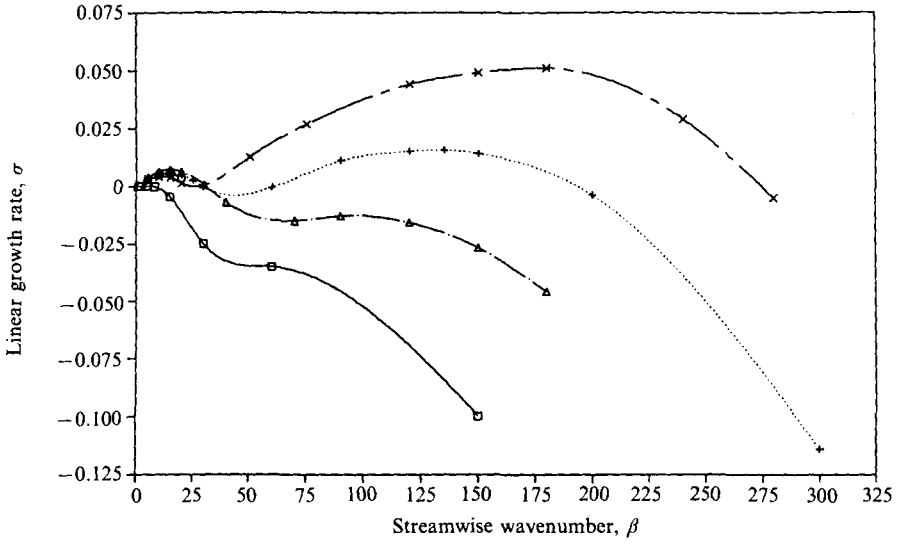

FIGURE 11. Same as figure 9 but with a larger range of β.

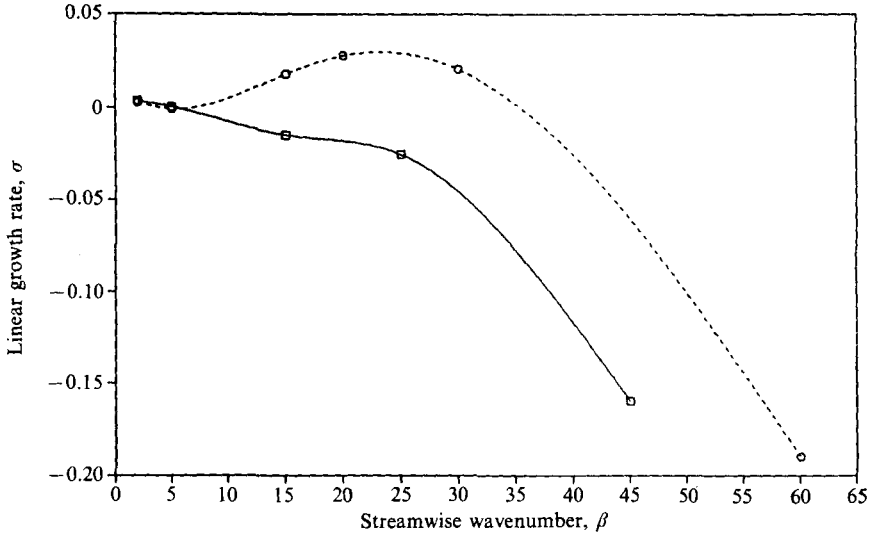

FIGURE 12. Linear growth rate, σ, of non-axisymmetric disturbances to Dean vortex flow at $a = 2.5$, $\eta = 0.875$ for $Re = 2.270Re_c$ (□), and $Re = 3.153Re_c$ (○).

vortices may occur. We also define Re_β as the Reynolds number at which $\sigma(\beta_u) = \sigma(\beta_t)$. By interpolation, $Re_\beta \approx 2.11Re_c$ and $Re''_{ns} \approx 1.96Re_c$ for $a = 2.5$, $\eta = 0.975$; Re_β and Re''_{ns} are functions of a and η. For Re sufficiently greater than Re_β, $\sigma(\beta_t) \gg \sigma(\beta_u)$. This behaviour provides the most significant difference between curved channel and Taylor–Couette flows.

Shown in figure 12 is $\sigma(\beta)$ for two Re with $a = 2.5$, $\eta = 0.875$; these are qualitatively similar to those in figure 11, for which $\eta = 0.975$. Both β_u and β_t scale roughly with the number of channel spacings in a circumference, i.e. the non-dimensional wavelengths $2\pi r_c/\beta_u$ and $2\pi r_c/\beta_t$ are nearly the same for both radius ratios. By interpolation, $Re''_{ns} \approx 2.58Re_c$ for $\eta = 0.875$, which is higher than for $\eta =$

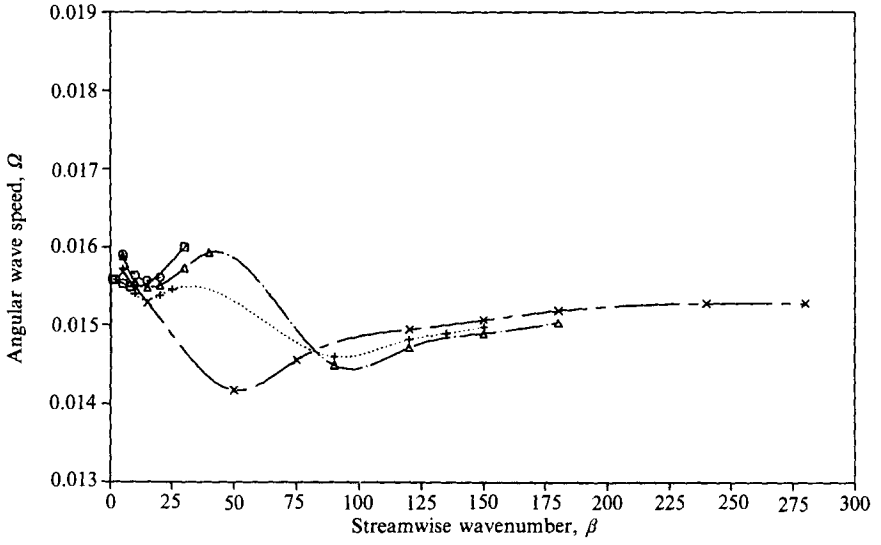

FIGURE 13. Same as figure 10 but with a larger range of β, and including $Re = 2.733Re_c$ ($\times$).

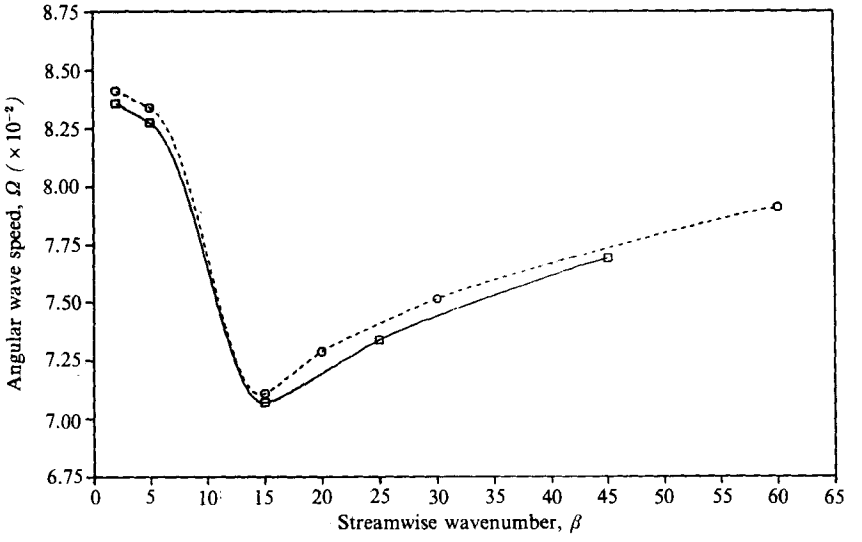

FIGURE 14. Angular wave speed Ω of small-amplitude non-axisymmetric disturbances to Dean vortex flow at $a = 2.5$, $\eta = 0.875$ for $Re = 2.270Re_c$ (□), and $Re = 3.153Re_c$ (○).

0.975; $Re_c = 52.4$ at $\eta = 0.875$. These results are in contrast to the nearly constant behaviour of Re/Re_c for transition to wavy Taylor vortices at these two η (Jones 1981).

The value of β observed experimentally depends on upstream conditions and linear growth rates. If the latter are dominant, then for $Re'_{ns} < Re < Re_\beta$ long-wavelength undulating vortices should occur, but for $Re \geqslant Re_\beta$ the short-wavelength twisting vortices should be found. For $Re'_{ns} < Re < Re''_{ns}$ only undulating vortices are possible. For $Re \approx Re_\beta$, $\sigma(\beta_u) \approx \sigma(\beta_t)$ and upstream conditions may determine which type of waviness occurs. Indeed, nonlinear runs with $Re \approx Re_\beta$ result in either undulating or twisting vortices, depending on initial conditions.

Near Re_β both types of waves could occur simultaneously. Nonlinear runs with $Re \approx Re_\beta$, with both types of waves well resolved and contained in initial conditions, did not yield mixed flows. For $Re \leqslant 8.199 Re_c$, the equilibrium state was always either pure undulating or pure twisting vortices.

The behaviour of the angular wave speed, Ω, as a function of β and Re is given in figure 13. The speeds of the two types of waves are nearly equal and are only weak functions of Re. For $Re > Re_\beta$ and large β in the range considered, $\Omega(\beta)$ is nearly constant. Figure 14 gives $\Omega(\beta)$ for two Re with $a = 2.5$, $\eta = 0.875$; comparing with figure 13, Ω decreases as η decreases. For both η, Ω is only weakly dependent on β and Re. For wavy Taylor vortices with $0.693 \leqslant \eta \leqslant 0.950$, King *et al.* (1984) found Ω decreased monotonically as η decreased.

6. Simulation of nonlinear non-axisymmetric vortices

In this section we examine nonlinear, non-axisymmetric solutions of the Navier–Stokes equations for $Re > Re'_{ns}$ and $\eta = 0.975$. Most of our results have $a = 2.5$; we choose this value because, experimentally, Kelleher *et al.* (1980) observed vortices with $a \approx 2.55$ and Hunt & Joubert (1979) observed $a \approx 2.17$.

6.1. *General remarks*

Fully developed wavy vortices are travelling waves in which the flow pattern travels with uniform angular velocity Ω. This is similar to the behaviour of wavy Taylor vortex flow. Specifically, the velocity satisfies the spatio–temporal property of a travelling wave (Rand 1982):

$$\boldsymbol{v}(r, (\theta + \Omega \Delta t) \bmod 2\pi/\beta, z, t + \Delta t) = \boldsymbol{v}(r, \theta, z, t). \tag{6.1}$$

In the literature on wavy Taylor vortices the alternative term 'rotating wave' is sometimes used. Setting $\Delta t = 0$ in (6.1) implies streamwise periodicity with wavenumber β; setting $\Delta t = 2\pi/(\Omega\beta)$ shows that the travelling wave has temporal periodicity with frequency $\omega = \Omega\beta$. In addition, wavy vortices have shift-and-reflect symmetry (cf. Marcus 1984):

$$\left.\begin{aligned} v_r(r, \theta, z, t) &= v_r(r, \theta + \pi/\beta, -z, t), \\ v_\theta(r, \theta, z, t) &= v_\theta(r, \theta + \pi/\beta, -z, t), \\ v_z(r, \theta, z, t) &= -v_z(r, \theta + \pi/\beta, -z, t), \end{aligned}\right\} \tag{6.2}$$

within roundoff error. The strengths of the travelling waves grow with Re.

We define $E^{(z)}(k_z)$ as the sum of the energy of all modes with spanwise wavenumber $\pm k_z$:

$$E^{(z)}(k_z) = c(k_z) \int_{r_i}^{r_o} \sum_{l=0}^{L} c(k_\theta) [|\hat{\boldsymbol{v}}(r, k_\theta, k_z, t)|^2 + |\hat{\boldsymbol{v}}(r, k_\theta, -k_z, t)|^2] \, \mathrm{d}r, \tag{6.3}$$

where $c(k)$ is given by (3.7), and $\hat{\boldsymbol{v}}(r, k_\theta, k_z, t)$ is the Fourier transform of the velocity, given by (2.1). We have used (2.3) to account for modes with $k_\theta < 0$. Similarly, the energy of the $\pm k_\theta$ modes is defined by

$$E^{(\theta)}(k_\theta) = c(k_\theta) \int_{r_i}^{r_o} \sum_{m=0}^{M} c(k_z) [|\hat{\boldsymbol{v}}(r, k_z, k_\theta, t)|^2 + |\hat{\boldsymbol{v}}(r, -k_z, k_\theta, t)|^2] \, \mathrm{d}r. \tag{6.4}$$

For equilibrium-state travelling waves, $E^{(k_z)}$ and $E^{(k_\theta)}$ are time independent.

As in wavy Taylor vortex flow (Marcus 1984), $\ln E^{(z)}(k_z)$ and $\ln E^{(\theta)}(k_\theta)$ are linear in

$|k_z|$ and $|k_\theta|$, except when $|k_z|$ is near a or $|k_\theta|$ is near β. In §3.1 we gave an explanation for the linear behaviour of $\ln E^{(z)}(k_z)$ for axisymmetric vortices. The argument used there can be applied directly to $\ln E^{(z)}(k_z)$ for the non-axisymmetric case, and to $\ln E^{(\theta)}(k_\theta)$ by replacing all references to z with θ and realizing that energy transfer occurs from the mean pressure gradient only to the $k_z = k_\theta = 0$ mode. With increasing $|k_z|$, $\ln E^{(z)}(k_z)$ drops less rapidly for wavy vortices than for the corresponding axisymmetric vortices at the same a, Re, η. We monitor the adequacy of the spatial resolution by observing whether $\ln E^{(z)}(k_z)$ and $\ln E^{(\theta)}(k_\theta)$ are linear up to the maximum $|k_z|$ and $|k_\theta|$ allowed.

Wavy vortices are temporally periodic, so temporal power spectra contain energy only in integer multiples of the fundamental frequency, ω. We simulate the spectra obtained by a probe that moves at constant angular velocity, Ω_p, in the streamwise direction. We find that such 'flying hot wire' spectra have ω shifted by an amount equal to $\beta\Omega_p$; all frequencies with non-zero energy are integer multiples of the shifted fundamental frequency. This demonstrates that wavy Dean vortex flow is a travelling wave. That the waviness is a travelling wave is also justified by Theorem 1 of Rand (1982), who showed for certain curved flows that if a stationary axisymmetric state (e.g. Dean vortex flow) bifurcates to a non-axisymmetric time-dependent state that is an attracting periodic orbit (e.g. wavy Dean vortex flow), the new time-dependent state must be a travelling wave.

In the curved channel, the speed of all travelling waves we observe is less than the maximum streamwise fluid velocity, i.e. $r\Omega < \max_{r,\theta,z} v_\theta(r,\theta,z,t)$. At a given instant there are two surfaces on which v_θ is equal to the speed of the travelling wave. For wavy Taylor vortices there is only one such surface; for Taylor vortices that are neutrally stable to non-axisymmetric disturbances with given β, Marcus (1984) finds that the 'comoving surface' associated with the speed of a wave with this β passes through the vortex centres. In the curved channel, we find that neither comoving surface passes through the vortex centres.

6.2. *Flow features*

We now consider some wavy Dean vortex velocity fields. Shown in figure 15 are arrow plots of the cross-flow velocities for undulating Dean vortex flow with $Re = 1.776Re_c$, $a = 2.5$, $\beta = 15 \approx \beta_u$. The resolution is $63 \times 33 \times 19$ (the number of modes in θ, r, z). The spatial grid has $\frac{3}{2}$ this resolution in each direction (cf. §2) but, for visual clarity, not all points in the grid are shown. The plots represent the cross-flow velocities for a sequence of (r,z)-planes. The streamwise flow is perpendicular to and out of the plane of the plots. Only half a streamwise wavelength is shown, since the other half of the sequence can be obtained from the shift-and-reflect property (6.2). Since the flow is a travelling wave, figure 15 is equivalent to a temporal sequence of the cross-flow velocities at one streamwise location. The spanwise locations of the vortex centres oscillate considerably. At each θ, one of the vortices in the pair is weakened, while the other is strengthened. This flow bears remarkable resemblance to the wavy Taylor vortices shown in figure 6 of Marcus (1984) for Taylor–Couette parameters that correspond to the curved channel flow parameters $Re = 2.063Re_c$, $\beta = 6$, $a = 1.047$, $\eta = 0.875$.

Arrow plots of the cross-flow velocities for twisting vortices with $Re = 2.186Re_c$, $a = 2.5$, $\beta = 135 \approx \beta_t$ are shown in figure 16; $95 \times 33 \times 19$ resolution was used. The streamwise wavelength is $\frac{1}{9}$ that of the undulating solution shown in figure 15. Again, only half a streamwise wavelength is shown. In contrast to undulating flow, the spanwise locations of the vortex centres in figure 16 oscillate only a little. For each

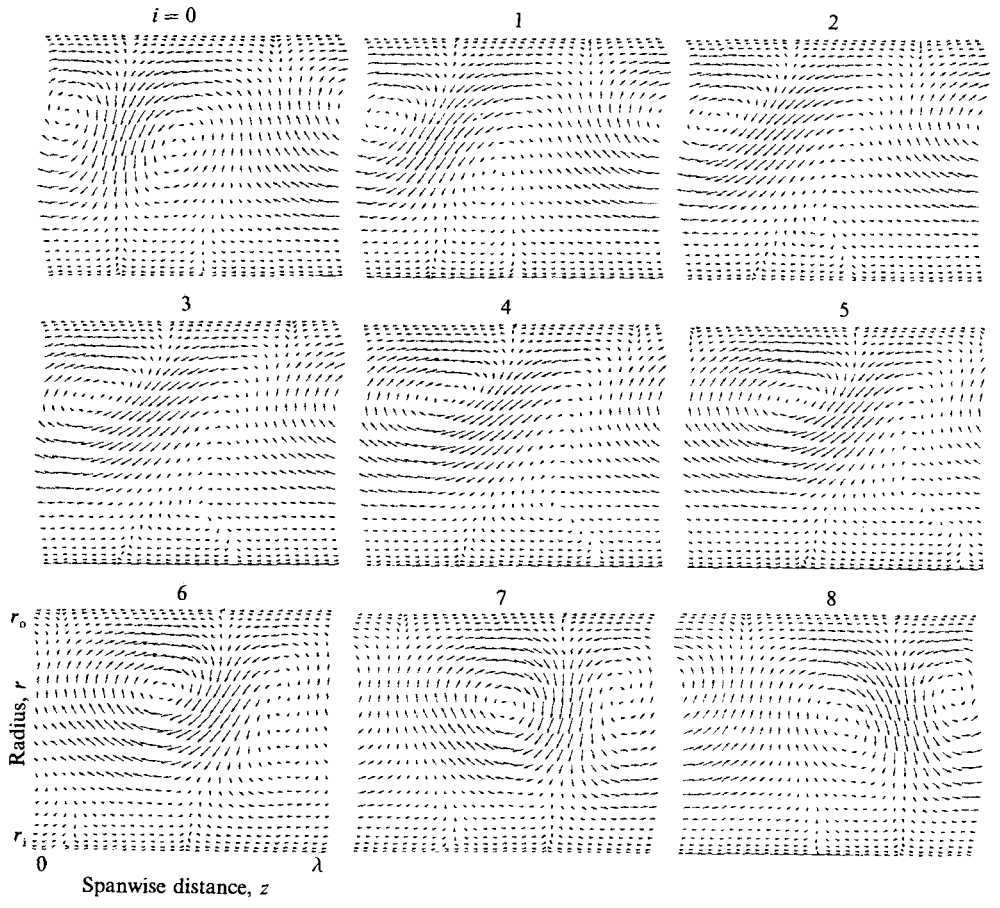

FIGURE 15. Undulating Dean vortex flow at $Re = 1.776Re_c$, $a = 2.5$, $\beta = 15$, $\eta = 0.975$ projected onto (r,z)-planes for $\theta = (2\pi/\beta)(i/16)$, $i = 0, 1, 2, \ldots, 8$. All nine plots have axes as given in the $i = 6$ plot. Plots for $9 \leqslant i \leqslant 16$ are a reflection about $z = \frac{1}{2}\lambda$ of the plot at $i-8$.

θ, one of the vortices in figure 6 appears more rectangular and weakened, while the other is more circular and strengthened.

Contours of u_θ, v_r and v_z associated with figures 15 and 16 are given in Finlay *et al.* (1987*a*). The cross-flow velocities distort the CCPF velocity profile by momentum transport to and from the walls, as discussed in §3 for axisymmetric vortices.

Examining figure 16 and contour plots of streamwise vorticity, it is shown that as θ increases, the radial position of a twisting vortex moves closer to the inner wall when the vortex is strong and moves outward when the vortex is weak. Because there are strong (θ, z) shear layers at both walls, and (r, θ) shear layers between the vortices (cf. §8), vortex lines do not just form tubes centred around the Dean vortices. However, by examining vorticity and velocity fields and vortex lines for these flows, we find that the only vortical structures are the streamwise-oriented Dean vortices; all other vorticity is associated with the shear layers just mentioned.

In Taylor–Couette flow experiments, the inflow and outflow regions of wavy vortices are visualized by suspending reflecting flakes in the fluid. These flakes align with the direction of flow, and variations in their orientation are observed as variations in transmitted or reflected light intensity (cf. DiPrima & Swinney 1985).

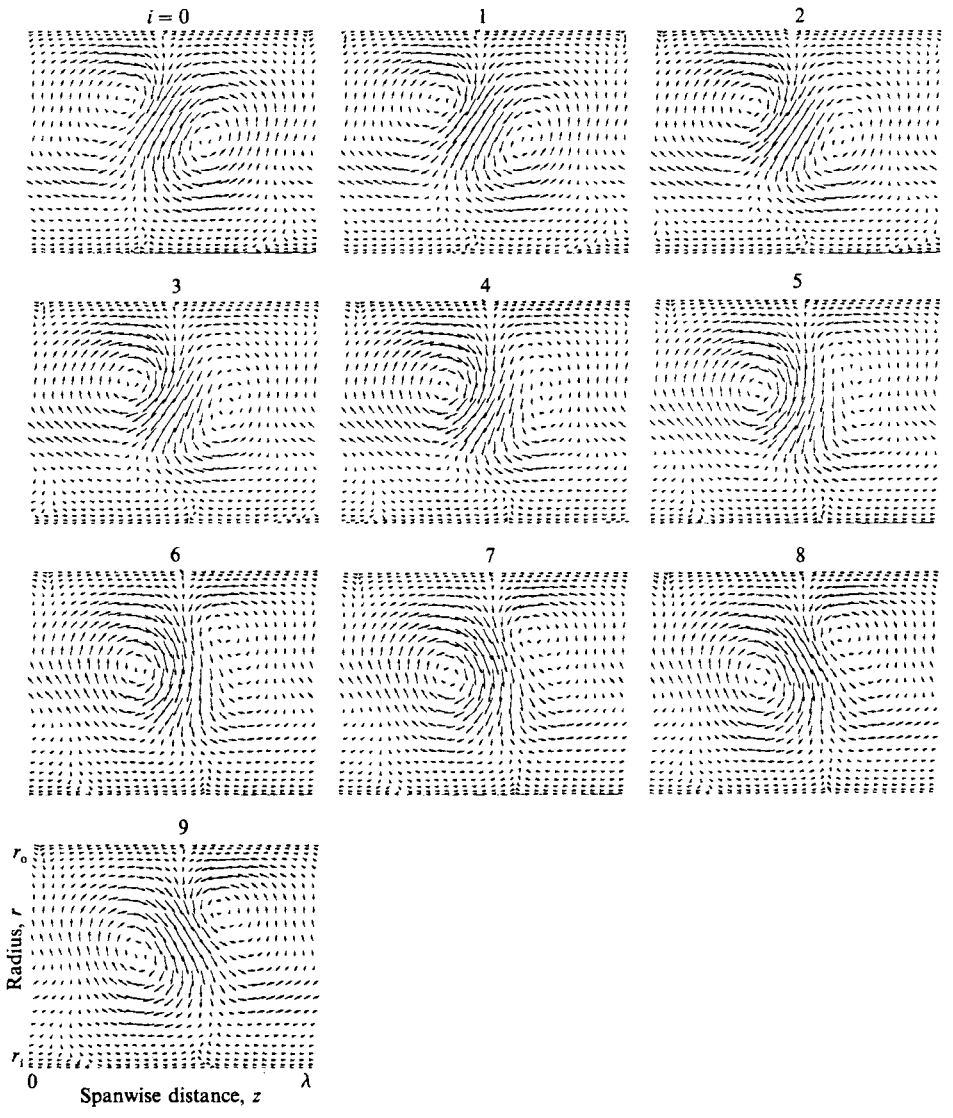

FIGURE 16. Twisting Dean vortex flow at $Re = 2.186Re_c$, $a = 2.5$, $\beta = 135$, $\eta = 0.975$ projected onto (r, z)-planes for $\theta = (2\pi/\beta)(i/18)$, $i = 0, 1, 2, \ldots, 9$. All ten plots have axes as given in the $i = 9$ plot. Plots for $10 \leqslant i \leqslant 18$ are a reflection about $z = \frac{1}{2}\lambda$ of the plot at $i-9$.

To reproduce the qualitative features of such a flow visualization from numerical simulation data, Marcus (1984) evaluated

$$B(\theta, z) \equiv \int_{r_i}^{r_o} v_r^2/(v_\theta^2 + v_z^2)\,\mathrm{d}r;$$

B is largest in inflow and outflow regions, although the experimental flow visualization does not correspond to a well-defined mathematical quantity. In figure 17 we plot lines through the two peaks of B for undulating vortices at $Re = 1.776Re_c$, $\beta = 15$ and $a = 2.5$. Two streamwise wavelengths are shown. The higher peak of B corresponds to the inflow region. The much lower peak of B near the outflow region is nearly discontinuous at two values of θ per streamwise wavelength.

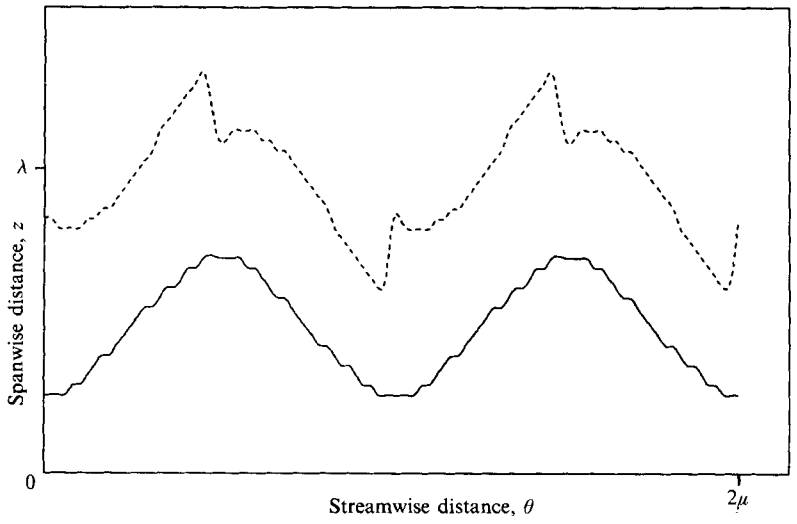

FIGURE 17. The line drawn through the higher peak of $B(\theta, z) \equiv \int_{r_i}^{r_o} v_r^2/(v_\theta^2+v_z^2)\,dr$ for undulating Dean vortex flow at $Re = 1.776Re_c$, $a = 2.5$, $\beta = 15$, $\eta = 0.976$. (——) corresponds approximately with the inflow boundary. See text for explanation of line through lower peak of B (– – –).

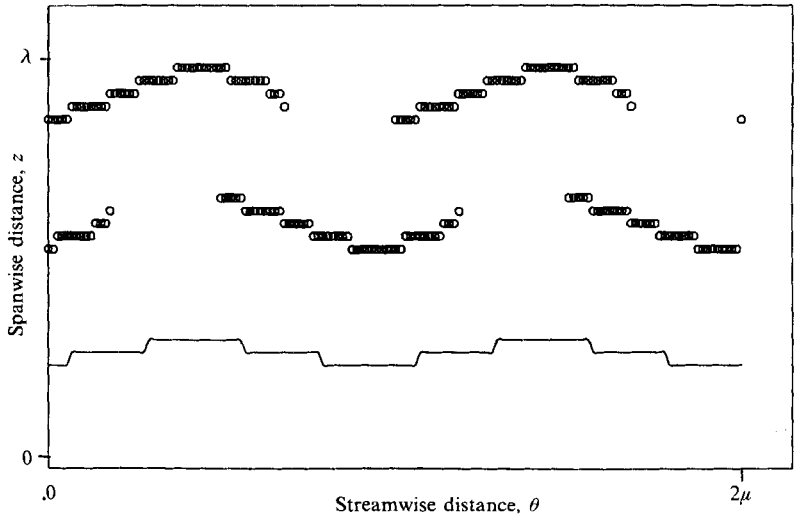

FIGURE 18. Approximate inflow boundary (——) for twisting Dean vortex flow at $Re = 2.186Re_c$, $a = 2.5$, $\beta = 135$, $\eta = 0.975$ determined from B, which is defined in figure 17. B has two local peaks (○) near the outflow region and is not useful in determining an outflow boundary.

Discontinuities are not observed in the velocity flow field (cf. figure 15). With the exception of these discontinuities, the outflow region corresponds roughly with this peak of B, although figure 15 gives a better idea of the position of the outflow region.

In wavy Taylor vortex experiments, the spanwise displacement of the inflow region is larger than that of the outflow region. In addition, the maximum spanwise deflections of the two regions occur at quite different values of θ (e.g. the inflow and outflow regions appear out of phase in θ by nearly $\frac{1}{3}\,2\pi/\beta$ in Marcus 1984). These

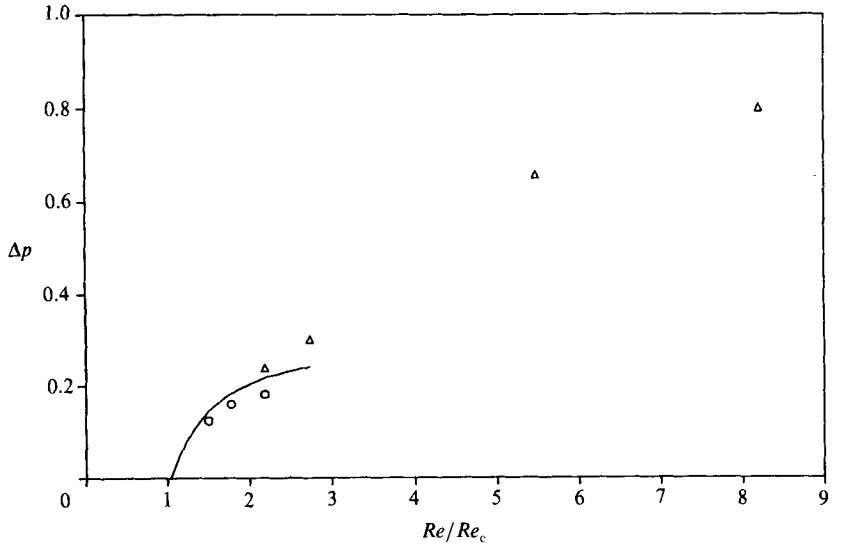

FIGURE 19. Δp versus Re for Dean vortex flow (——), undulating Dean vortex flow (○), and twisting Dean vortex flow (△), at $a = 2.5$, $\eta = 0.975$. The values of β for the undulating Dean vortex flow points are $\beta = 13, 15, 15$ corresponding to $Re/Re_c = 1.503, 1.776, 2.186$. The twisting Dean vortex flow points have $\beta = 135, 180, 200, 200$ corresponding to $Re/Re_c = 2.186, 2.733, 5.466, 8.199$.

features are not apparent in undulating Dean vortex flow. In contrast to wavy Taylor vortices, the inflow region for wavy Dean vortices has larger cross-flow velocities than the outflow region.

For twisting vortices, the parameter B is not useful in determining an approximate outflow boundary, because at some streamwise locations B has two peaks near the outflow region, in addition to the single peak at the inflow region. Figure 18 shows the peaks of B for twisting Dean vortex flow at $Re = 2.186Re_c$, $\beta = 15$ and $a = 2.5$. Two streamwise wavelengths are shown. Examining figure 16, we see that for this flow the outflow region is quite wide in z, with large radial velocities occurring at two separate locations near the outflow sides of both vortices. This leads to two peaks in B near the outflow region. As for undulating vortices, and in contrast to wavy Taylor vortex flow, the points of maximum spanwise deflection of the inflow/outflow regions occur at roughly the same streamwise location.

The two types of waviness differ from each other in their effect on Δp (cf. (3.3)). For undulating vortices Δp is lower than for (unstable) axisymmetric vortices at the same Re, a, η. This is similar to Taylor–Couette flow in which wavy Taylor vortices have lower torque than the axisymmetric vortex flow. In contrast, twisting vortices cause higher Δp than the corresponding unstable Dean vortex flow. Shown in figure 19 are values of Δp as a function of Re at $a = 2.5$ for axisymmetric vortices and for several wavy solutions with β near β_u or β_t.

For $Re \geqslant 2.733Re_c$ we examined solutions having $\beta \geqslant 180$, where linear growth rates of non-axisymmetric disturbances are greatest. For $Re \geqslant 2.733Re_c$, $\sigma(\beta_t) \gg \sigma(\beta_u)$ (cf. §5), and in the absence of nonlinear wavelength selection mechanisms, twisting vortices occur.

Twisting vortex flow at $Re = 2.733Re_c$, $a = 2.5$, $\beta = 180$ is similar to that at $Re = 2.186Re_c$, $a = 2.5$, $\beta = 135$ discussed earlier. The cross-flow velocities of a twisting wave solution at $Re = 5.466Re_c$, $a = 2.5$, $\beta = 200$ are shown in figure 20; $95 \times 33 \times 35$

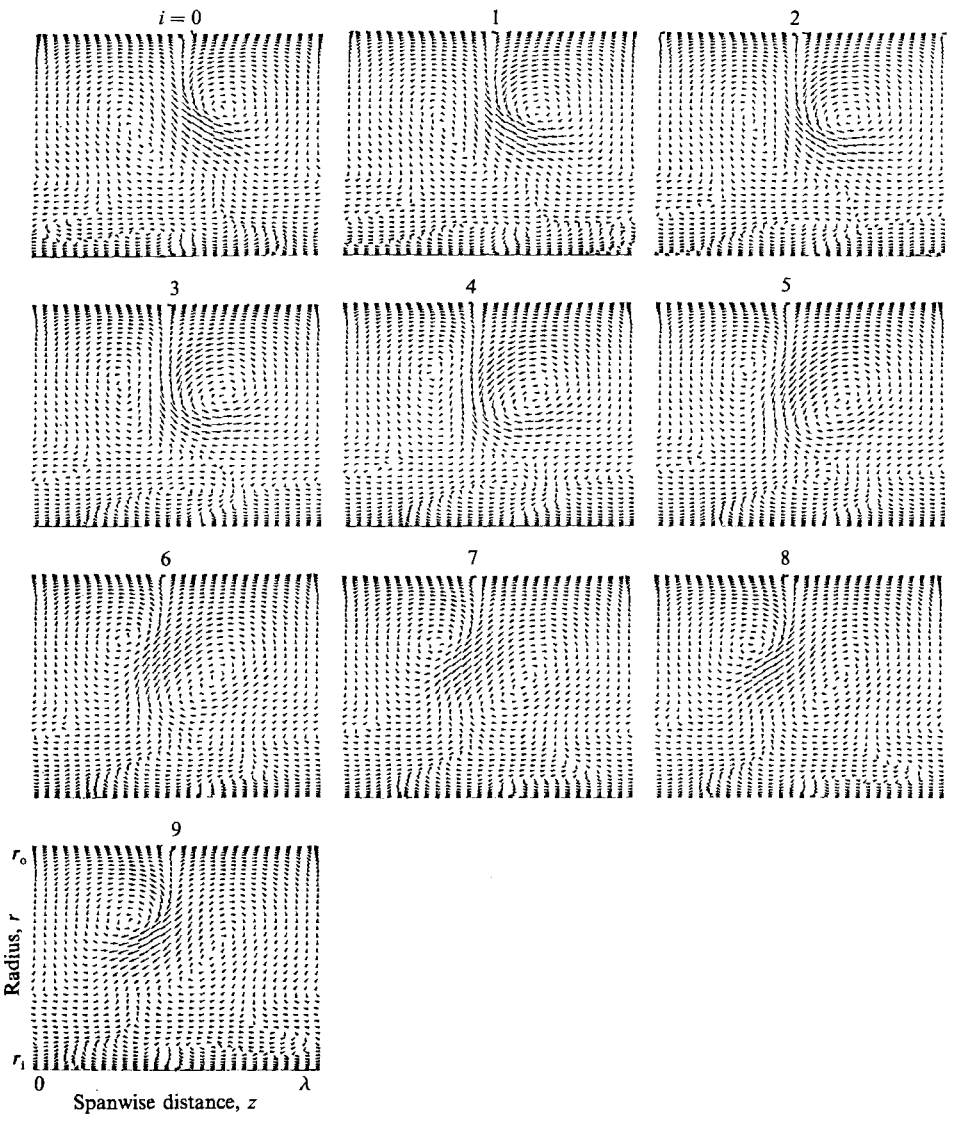

FIGURE 20. Twisting Dean vortex flow at $Re = 5.466Re_c$, $a = 2.5$, $\beta = 200$, $\eta = 0.975$ projected onto (r, z)-planes for $\theta = (2\pi/\beta)(i/18)$, $i = 0, 1, 2, \ldots, 9$. All ten plots have axes as given in the $i = 9$ plot. The velocity represented by an arrow in figure 16 would appear $\frac{1}{4}$ as long if drawn in this figure.

resolution was used. The vortex boundaries are contorted in the (r, z)-planes shown in figure 20. Oscillation of the inflow jet's direction causes a more complex flow near the inner wall than at lower Re. Contour plots of u_θ, v_r and v_z are given in Finlay *et al.* (1987*a*). As at lower Re, the cross-flow velocities distort the streamwise velocity. As Re increases, the cross-flow velocities and, therefore, the distortion increase. The flow at $Re = 8.199Re_c$, $a = 2.5$, $\beta = 200$ with $127 \times 33 \times 39$ resolution is similar to the flow at $Re = 5.466Re_c$, $a = 2.5$, $\beta = 200$.

Let

$$V_\theta(r) \equiv \frac{1}{\lambda\mu} \int_0^\lambda \int_0^\mu v_\theta(r, \theta, z, t)\, \mathrm{d}\theta\, \mathrm{d}z$$

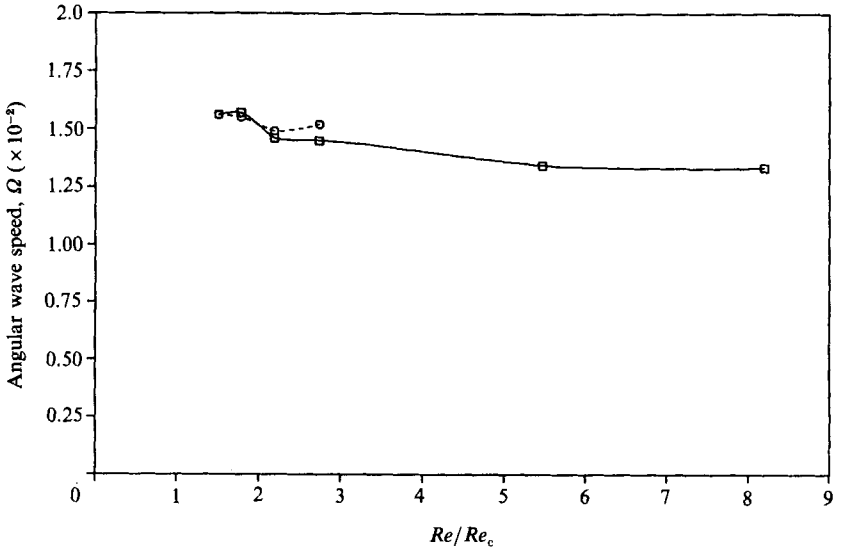

FIGURE 21. The angular wave speed Ω as a function of Re at $a = 2.5$, $\eta = 0.975$ for nonlinear wavy Dean vortex flow (□, ——) compared to the value for the small-amplitude travelling waves of §5 (○, – – – –). The values of β used for both curves are $\beta = 13, 15, 135, 180, 200, 260$, corresponding to $Re/Re_c = 1.503, 1.776, 2,186, 2.733, 5.466, 8.199$.

be the spanwise–streamwise average of v_θ for a travelling wave flow, and $\bar{L}(r) \equiv rV_\theta(r)$ be the mean streamwise angular momentum profile. For sufficiently large Re, $\bar{L}(r)$ is nearly constant except near the walls where boundary layers occur (cf. Finlay *et al.* 1987*a*).

Shown in figure 21 as a function of Re, and with $a = 2.5$, are values of the angular wave speed, $\Omega = \omega/\beta$, for wavy vortices. For $Re \leqslant 2.733Re_c$ the value of β used is not constant; it is near β_u for the undulating vortex flows, and near β_t for the twisting flows. For large $Re \leqslant 8.199Re_c$ the angular speed of the travelling wave is only a weak function of Re. For wavy Taylor vortices, $\Omega(Re)$ curves have a plateau for a range of Re (King *et al.* 1984). In figure 21 the flat region near the upper values of Re in the $\Omega(Re)$ curves may be part of such a plateau. For comparison, we include the values of Ω for the small-amplitude travelling waves of §5; these values are near those for nonlinear waves, as is the case for wavy Taylor vortex flow (Jones 1981).

In a run with $Re = 10.931Re_c$, $a = 2.5$, $\beta = 200$ and the $Re = 8.199Re_c$ velocity field as initial condition, a vortex-doubling bifurcation of the type discussed in §3 occurred. When the single vortex pair solution from $Re = 1.776Re_c$, $a = 2.5$, $\beta = 15$ was used as initial condition for $Re = 1.776Re_c$, $a = 1.5$, $\beta = 10$, a similar vortex doubling occurred. The discussion on axisymmetric vortex bifurcations in §3 is applicable to the non-axisymmetric case; an Eckhaus stability boundary may be present.

A second fundamental frequency, ω_2, appears as a transient in the early part of twisting vortex runs. While ω_2 is present, the flow is quasi-periodic, since ω and ω_2 are incommensurate frequencies. The energy in ω_2 eventually dies out, leaving the periodic travelling wave that is twisting flow. All flows, with or without ω_2, obey the shift-and-reflect symmetry property (6.2). Simulations of spectra obtained in moving reference frames show ω_2 to be a decaying non-propagating oscillatory mode, and not

a travelling wave. The nature of this mode is discussed in Finlay *et al.* (1987*a*). For $Re > 5Re_c$ in their Taylor–Couette experiment with $\eta = 0.877$, Fenstermacher, Swinney & Gollub (1979) observed a transient frequency, ω_2, with features similar to the one we observe.

7. Experimental wavy Dean vortex flow

To the authors' knowledge, other than Finlay *et al.* (1987*b*) the only published mention that Dean vortices are wavy at high Re is the comment by Kelleher *et al.* (1980): 'Observations of the flow patterns at much higher Reynolds number' ($Re \approx 3.44Re_c$, M. D. Kelleher 1986, private communication) 'indicated that the flow took on a streamwise periodicity in the form of longitudinal waves superposed on the secondary flow which would travel down the vortices in the direction of flow'. The waves had $\beta \approx 200$ (M. D. Kelleher 1986, private communication). All data presented by Kelleher *et al.* (1980) is for a rectangular channel with $\Gamma = 40$, $Re''_{ns} < 2.14Re_c \leqslant Re \leqslant 3.07Re_c$, $a \approx 2.55$, $\eta = 0.979$. The data in figures 4–6 of Kelleher *et al.* (1980) were obtained with a hot wire oriented parallel to the z-axis by slowly moving a hot wire across the channel in the z-direction at several radii 135° from the start of curvature. High-frequency oscillations appear in the hot-wire signal of figure 6 of Kelleher *et al.* (1980) taken at $Re = 3.07Re_c$. (Our runs with Re up to $8.199Re_c$ never become turbulent.) The time taken by their probe to cross one vortex pair was much less than any travelling wave period, so the signal due to a travelling wave would appear as a high-frequency oscillation. Based on linear growth rates at $Re = 3.07Re_c$, therefore, we suggest that the data of Kelleher *et al.* (1980) at $Re = 3.07Re_c$ represent a twisting vortex flow. At $Re = 2.14Re_c$ and $Re = 2.57Re_c$, rapid oscillations are not readily visible in their hot-wire signal, probably because their recording station is too far upstream for wavy disturbances of sufficient amplitude to have developed from upstream conditions.

7.1. *Streamwise development*

The following analysis provides qualitative estimates of the streamwise development of vortices and travelling waves. We assume that the flow at the entrance to the curved section ($\theta = 0$) is CCPF with small-amplitude disturbances. Most experimental curved channels have a plane channel section leading into the curved section, so the entrance flow is actually plane Poiseuille flow; however, CCPF is similar to plane Poiseuille flow for η sufficiently near unity.

First, consider the streamwise development of Dean vortices. At given Re, a, η an approximation to the flow is obtained at each θ by considering the weakly nonlinear solution of §4. This solution is axisymmetric and has time behaviour $A(t)$ (cf. Drazin & Reid 1981), where A obeys the Landau equation given by dropping terms higher than $O(A^3)$ in (4.9). Streamwise development of the flow can be approximated with temporal evolution of the weakly nonlinear solution by assuming that

$$t = \frac{r_c \theta}{\bar{U}}, \tag{7.1}$$

i.e. that the flow seen by an observer moving at the mean velocity is the same as the temporally developing flow. Substituting this into the solution of the Landau

equation, $A(t)$, we obtain the following approximation for the vortex amplitude normalized by its fully developed value, A_f:

$$\frac{A}{A_f} = \frac{A_0}{A_f}\left\{\left(\frac{A_0}{A_f}\right)^2 + \left[1-\left(\frac{A_0}{A_f}\right)^2\right]\exp\left(-\frac{2\sigma r_c\theta}{\bar{U}}\right)\right\}^{-\frac{1}{2}}. \tag{7.2}$$

Here, $A_0 \equiv A(0)$ and σ is the linear growth rate from §4. Based on our assumption of slightly perturbed CCPF at $\theta = 0$, we assume $A_0^2 \gg A_f^2$ and write (7.2) as

$$\frac{A}{A_f} \approx \left[1+\left(\frac{A_f}{A_0}\right)^2\exp\left(-\frac{2\sigma r_c\theta}{\bar{U}}\right)\right]^{-\frac{1}{2}}. \tag{7.3}$$

From (7.3) we see that changing the amplitude of the solution at $\theta = 0$ to A_0' yields

$$\frac{A}{A_f}\left(\theta, \frac{A_0'}{A_f}\right) = \frac{A}{A_f}\left(\theta-\theta', \frac{A_0}{A_f}\right), \tag{7.4}$$

where

$$\theta' = \frac{\bar{U}}{\sigma r_c}\ln\frac{A_0'}{A_0}. \tag{7.5}$$

Therefore we need to consider (7.3) with only one value of A_0/A_f, since A/A_f for other values can be obtained using (7.4) and (7.5).

To estimate A_0/A_f, we use the weakly nonlinear result given in (4.18) to obtain

$$\left(\frac{A_f}{A_0}\right)^2 = \frac{\Delta p_f}{\Delta p_0}, \tag{7.6}$$

where Δp_0 is the pressure-gradient parameter at $\theta = 0$, and Δp_f is the fully developed value. Within the $O(A^2)$ accuracy of the weakly nonlinear approximation we also have

$$\Delta p_0 = \frac{E_f(2\pi/a)}{E_0(2\pi/a)}\Delta p_f, \tag{7.7}$$

which is obtained using (3.6), (4.2), (4.5) and (4.7); E_f and E_0 are the final and initial values of $E(k_z)$ given in (3.6). In the range of Re, a, η considered in this section, the weakly nonlinear solution has streamwise perturbation velocity much greater than its radial or spanwise velocity, so we may approximate $E_0(2\pi/a)$ as follows. If we define

$$\frac{u'}{\bar{U}} \equiv \lim_{T\to\infty}\frac{a}{T\pi}\int_0^{\lambda}\int_{r_i}^{r_o}\int_0^{T} u_\theta(r,\theta=0,z,t)\cos az\,\mathrm{d}t\,\mathrm{d}r\,\mathrm{d}z, \tag{7.8}$$

where $u_\theta \equiv v_\theta - V$ is the streamwise perturbation velocity, then

$$\frac{u'}{\bar{U}} \approx \left[2E_0\left(\frac{2\pi}{a}\right)\right]^{\frac{1}{2}}. \tag{7.9}$$

For a good quality wind tunnel we might expect $u' \approx 0.1\,\%\bar{U}$; from full simulations with $a = 2.5$, $\eta = 0.975$ and $1.230Re_c \leqslant Re \leqslant 2.733Re_c$ we find $E_f(2\pi/a) \approx 0.01$ and $0.0788 \leqslant \Delta p_f \leqslant 0.240$, so that (7.7) implies $\Delta p_0 \approx 10^{-5}$. Using this value of Δp_0 and knowing Δp_f, we use (7.6) in (7.2) to evaluate A/A_f. Figure 22 shows A/A_f as a function of θ at various Re for $a = 2.5$, $\eta = 0.975$. Increasing Re causes the position at which the vortices are fully developed to move upstream; the value of θ at this

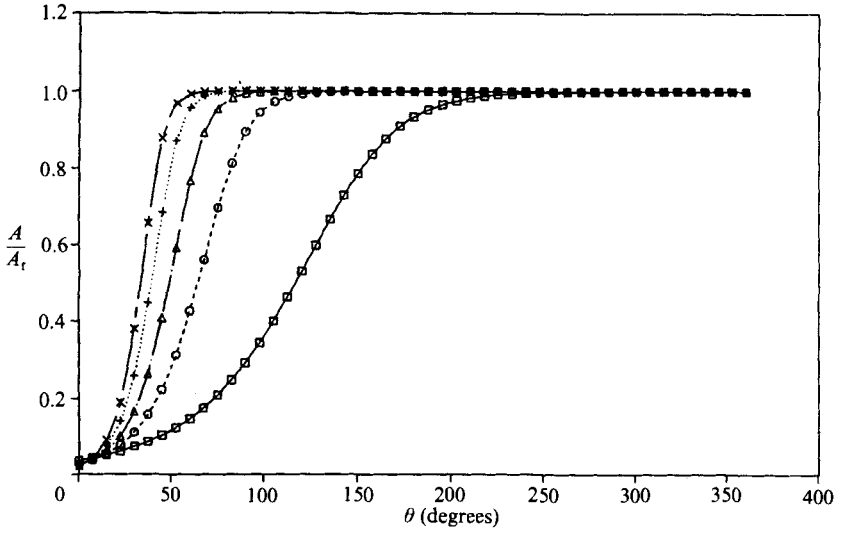

FIGURE 22. Amplitude A of weakly nonlinear Dean vortex solution, relative to steady state value A_f, as a function of streamwise position ($\theta = \bar{U}t/r_c$); for $a = 2.5$, $\eta = 0.975$ and various Re: □, $Re = 1.230Re_c$; ○, $1.503Re_c$; △, $1.776Re_c$; +, $2.186Re_c$; ×, $2.733Re_c$.

position approaches a constant for large Re. Based on (7.4) and (7.5), the curves for a different initial pressure-gradient parameter, $\Delta p_0'$, (see figure 24) can be obtained from figure 22 by shifting each curve to the left by an amount

$$\theta' = \frac{\bar{U}}{2\sigma r_c} \ln \frac{\Delta p_0'}{\Delta p_0}. \tag{7.10}$$

Now consider the development of wavy perturbations of Dean vortices. We assume the waviness is the result of a supercritical Hopf-type bifurcation, so that the amplitude of the wavy disturbance obeys a Landau equation. We then relate temporal growth with streamwise development and proceed in the same manner as for Dean vortices. For given Re, a, η, we define θ_0 as the position at which the flow becomes unstable to wavy disturbances. (Because CCPF is stable to small-amplitude wavy disturbances for the Re considered here, such disturbances will not amplify until Dean vortices of sufficient amplitude have developed.) We assume wavy disturbances grow from small-amplitude A_0 at θ_0 to their final amplitude A_f in the manner given by (7.2) with θ replaced by $\theta - \theta_0$ and σ interpreted as either $\sigma(\beta_u)$ or $\sigma(\beta_t)$ from §5. To obtain A_0/A_f for wavy disturbances, we use $\Delta p_0 = 10^{-5}$ in (7.6) and interpret Δp_f as the magnitude of the difference between Δp for the non-axisymmetric and (unstable) axisymmetric equilibrium state solutions. The value of A/A_f for travelling waves is shown in figure 23 as a function of θ at several Re for $a = 2.5$, $\eta = 0.975$. At each Re in this figure we arbitrarily assume θ_0 is the position where the inlet disturbances to CCPF have grown into Dean vortices with $A/A_f = 0.9$; using other θ_0 merely shifts the curves left or right. The curves with $Re \geqslant 2.186Re_c$ are for twisting vortices, and with $Re \leqslant 1.776Re_c$ are for undulating vortices. We see that fully developed undulating vortices may not occur within 360° of the inlet. Their development can be enhanced by artificially inducing large-amplitude waviness at θ_0. (We obtain undulating vortex solutions in a time $t < 2\pi r_c/\bar{U}$ by using a large-amplitude non-axisymmetric perturbation of axisymmetric vortices as initial

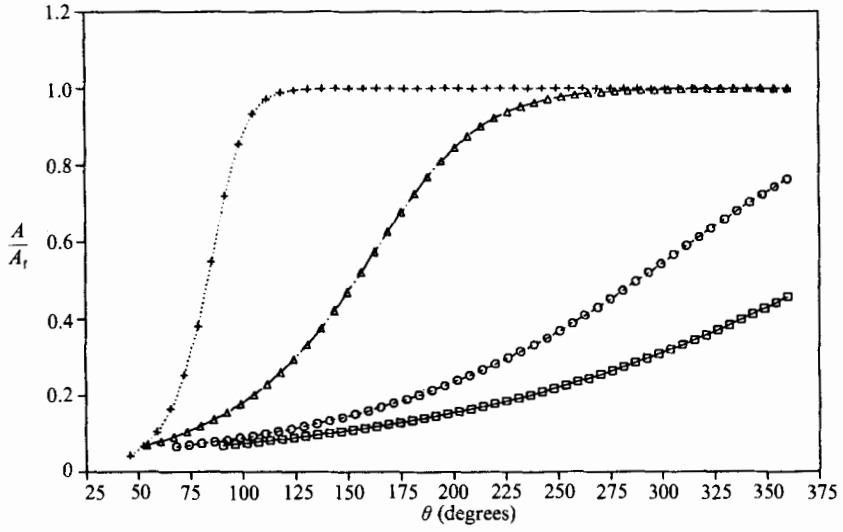

FIGURE 23. A/A_f of weakly nonlinear travelling wave, as a function of streamwise position ($\theta = \bar{U}t/r_c$); for $a = 2.5$, $\eta = 0.975$ and various Re: □, $Re = 1.230Re_c$; ○, $1.503Re_c$ (undulating waves); △, $1.776Re_c$; +, $2.186Re_c$ (twisting waves). We assume the travelling wave starts growing once $A/A_f = 0.9$ for Dean vortices.

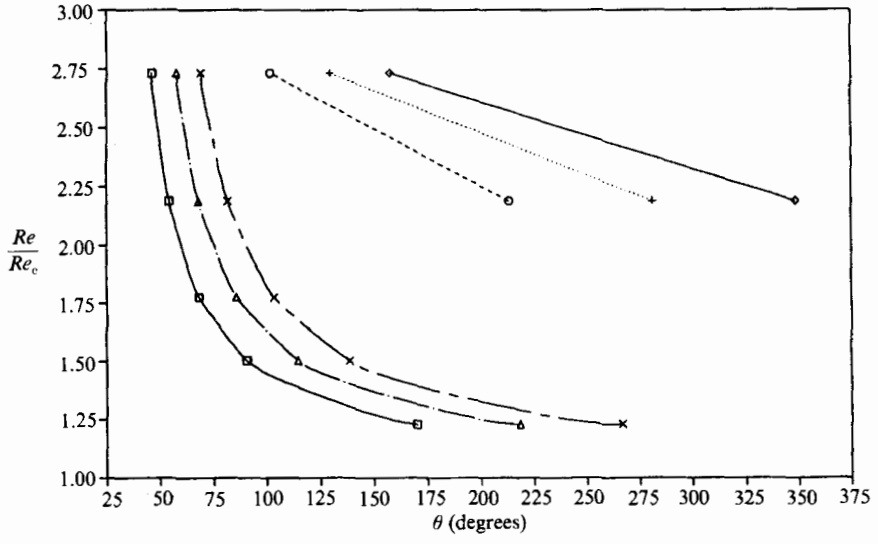

FIGURE 24. Streamwise position ($\theta = \bar{U}t/r_c$) at which weakly nonlinear Dean vortices and travelling waves have $A/A_f = 0.9$ for various values of Δp_0. Dean vortices: (□, ——) $\Delta p_0 = 10^{-4}$; (△, —·—) $\Delta p_0 = 10^{-5}$; (×, – – –) $\Delta p_0 = 10^{-6}$. Twisting wave: (○, – – –) $\Delta p_0 = 10^{-4}$, (+, ·····) $\Delta p_0 = 10^{-5}$, (◇, ——) $\Delta p_0 = 10^{-6}$.

condition.) The Re at which twisting vortices become apparent in an experiment for given a, η depends on the method of measurement and the upstream conditions. Figure 23 is in agreement with our earlier comments regarding the experiment of Kelleher *et al.* (1980), in which travelling waves of sufficient amplitude to be recorded by their hot wire at $\theta = 135°$ occurred when $Re = 3.07Re_c$, but not at the two lower Re.

Increasing the amplitude of the disturbances moves the stages of vortex development upstream. For example, shown in figure 24 as a function of Re, for several values of Δp_0, is the position at which $A/A_f = 0.9$. Based on (7.7)–(7.9), the range of Δp_0 shown corresponds approximately to $0.0004 \leqslant u'/\bar{U} \leqslant 0.004$. The effect of an increase in either the disturbance level or Re on the vortex development decreases as Re increases. Niver (1987) ($\eta = 0.979$, $\Gamma = 40$) found that 'moderate unsteadiness' developed in smoke visualizations at streamwise locations similar to those for twisting vortices in figure 24. We suggest this unsteadiness was caused by twisting waves.

For $\eta = 0.975$, these results indicate that a minimum distance of roughly $\frac{1}{4}\pi r_c$ is needed for the full development of Dean vortices from small-amplitude disturbances, and much longer lengths are required when $Re \approx Re_c$. Twisting vortices develop within a distance πr_c from the start of curvature if $Re > 2.5Re_c$, while fully developed undulating vortices may not occur within one circumference. Thus we expect that experiments with streamwise extent less than 180° would first see Dean vortices and then, at higher Re, twisting Dean vortices. This result is true for both η considered. It is consistent with the experiments of Kelleher *et al.* (1980) and Niver (1987), but is in contrast to the behaviour of Taylor–Couette flow in which the undulating mode dominates.

8. Instability mechanisms

Here, we propose shear instability as a mechanism for the development of twisting vortices. The streamwise perturbation velocity for Dean vortex flow is $u_\theta(r,z) = v_\theta(r,z) - V(r)$, where $V(r)$ is the CCPF velocity profile given in (3.1). At a given radius, u_θ usually has opposite sign at the inflow and outflow regions (cf. figure 3). Thus, v_θ as a function of z for given r must have two inflexion points near $z = \frac{1}{4}\lambda$ and $z = \frac{3}{4}\lambda$, where $z = 0$ is an inflow or outflow plane. Such a velocity profile may be unstable to shear instability.

We use terms to $O(A)$ in the weakly nonlinear approximation of $v_\theta(r,z)$ (cf. §4),

$$v_\theta(r,z) = V(r) + Av_{10}(r)\cos az + O(A^2), \tag{8.1}$$

to examine whether Dean vortices may be unstable in this manner. Because it is the inflexion points in $v_\theta(r,z)$ that are important for shear instability, we reduce the problem to one dimension, making it amenable to Orr–Sommerfeld-type analysis, by averaging (8.1) over r. (Neglecting the finite radial extent of the shear layer may be a severe approximation.) Keeping terms to $O(A)$, this yields

$$U(z) = 1 + \epsilon\cos az, \tag{8.2}$$

where

$$\epsilon = \tfrac{1}{2}A\int_{r_i}^{r_o} v_{10}(r)\,\mathrm{d}r$$

is a function of Re, a, η. We assume $\eta \approx 1$ in order to approximate the curved channel by a rectilinear one. We then perform a classical Orr–Sommerfeld analysis. Two-dimensional small-amplitude perturbations to the velocity profile $U(z)$ can be written in terms of a stream function:

$$\Psi(\theta,z,t) = \phi(z)\,\mathrm{e}^{\mathrm{i}\beta\theta}\,\mathrm{e}^{(\sigma-\mathrm{i}\omega)t}. \tag{8.3}$$

Equation (8.3) is a two-dimensional approximation to the three-dimensional small-amplitude disturbance given in (5.1). The interpretation of β, σ, ω is the same as in

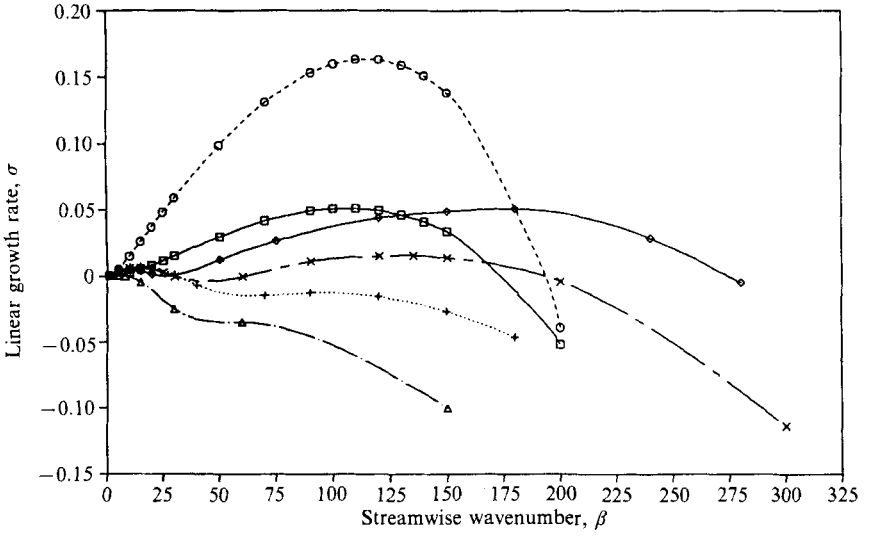

FIGURE 25. Linear growth rates of shear instability discussed in §8, at $Re = 1.264Re_c$ (□, ——), and $Re = 2.579Re_c$ (○, – – – –) compared to the linear growth rates of non-axisymmetric disturbances from §5: (△, —·—) $Re = 1.230Re_c$, (+, ·····) $Re = 1.776Re_c$, (×, – – – –) $Re = 2.186Re_c$, (◇, ——) $Re = 2.733Re_c$; at $a = 2.5$, $\eta = 0.975$.

(5.1). Making use of (8.3), we reduce the Navier–Stokes equations to the Orr–Sommerfeld equation with periodic boundary conditions. For given (Re, a, β, η) this is an eigenvalue problem for $\sigma - i\omega$ and the complex-valued eigenfunction $\phi(z)$, which we solve by a Galerkin approach; ϕ is expanded in a Fourier series as

$$\phi(z) = \sum_{n=0}^{M} d_n \cos naz + \sum_{n=1}^{M} e_n \sin naz. \tag{8.4}$$

The equations decouple into $M+1$ equations for the d_n, and M equations for the e_n (cf. Finlay *et al.* 1987*a*). As discussed in §5, a disturbance with all $e_n = 0$ is in phase, while a disturbance with all $d_n = 0$ is out of phase. We solved the eigenvalue problems using $M = 20$. For the range $Re \leqslant 2.733Re_c$, $\beta \leqslant 250$, $a = 2.5$ that we examine, $\sigma < 0$ for in-phase modes. Thus, as in §5, it is out-of-phase modes that determine stability. In figure 25, $\sigma(\beta)$ is given for out-of-phase modes at two Re with $a = 2.5$, $\eta = 0.975$. The linear growth rates obtained in §5, from the two-dimensional eigenvalue problem for non-axisymmetric disturbances, are included for reference. Each $\sigma(\beta)$-curve from the one-dimensional, Orr–Sommerfeld analysis has a single maximum. The value of β at this maximum is close to β_t (cf. §5); β_u is much smaller. Thus, Orr–Sommerfeld analysis suggests twisting vortices are due to a shear instability. The maximum linear growth rates found here are larger than those obtained in §5. In addition, the neutrally stable Reynolds number for twisting waves, Re''_{ns}, predicted by the one-dimensional analysis for $a = 2.5$, $\eta = 0.975$ is below the value obtained in §5. However, it is unreasonable to expect a one-dimensional analysis to duplicate more than the general features of the two-dimensional problem.

For $a = 2.5$, $\eta = 0.975$, the wave speed $\Omega = \omega/\beta$ given by Orr–Sommerfeld analysis for out-of-phase modes is independent of Re and β: $\Omega = 0.012658$, i.e. there is no dispersion. (Temporal, linear stability analysis of the free shear layer with velocity profile $U(z) = 0.5(1 + \tanh z)$ also predicts an absence of dispersion (Maslowe 1985).)

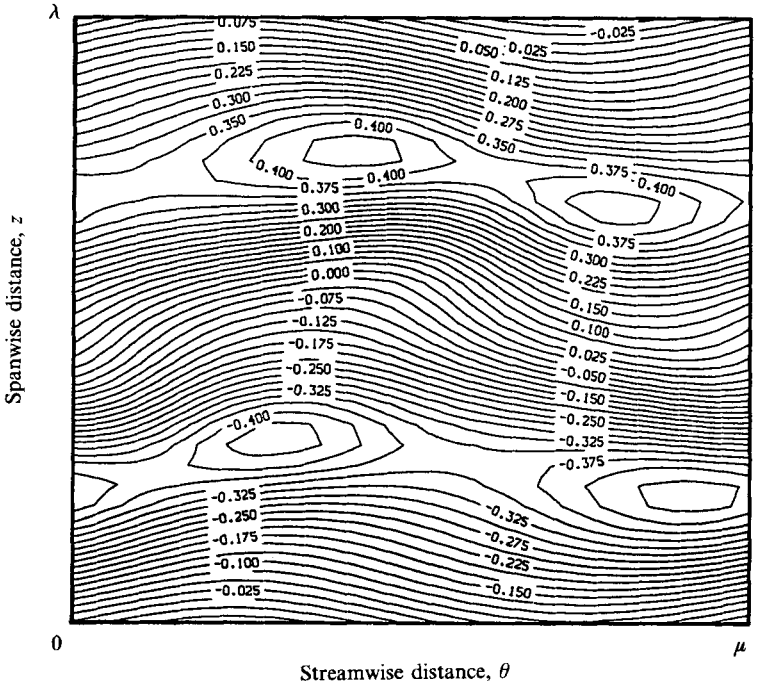

FIGURE 26. Contours of radial vorticity, ω_r, in (θ, z)-planes for twisting Dean vortex flow at $Re = 2.186Re_c$, $a = 2.5$, $\beta = 135$, $\eta = 0.975$, $r = r_c - \frac{1}{4}d$.

Recall that nonlinear wavy vortices are associated with a non-dispersive travelling wave. Travelling wave speeds for small-amplitude non-axisymmetric disturbances are found in §5 and are given for $\eta = 0.975$ in figure 13; the values of Ω predicted by one-dimensional shear instability analysis are near these wave speeds.

A characteristic of shear-layer instabilities is that a row of vorticity maxima or minima, depending on the orientation of the shear layer, develops along the line of inflexion points (Drazin & Reid 1981). If twisting waves develop from a shear instability, then in a (θ, z)-surface, we expect two rows of concentrations of radial vorticity, ω_r, per spanwise wavelength, one row consisting of positive vorticity and one of negative vorticity. The rows should be centred near the inflexion points of the velocity profile, at $z \approx \pm\frac{1}{4}\lambda, \pm\frac{3}{4}\lambda, \pm\frac{5}{4}\lambda, \ldots$, and should alternate in the spanwise direction. The existence of such vorticity extrema provides evidence that twisting vortex flow is due to shear instability. Shown in figure 26 are contours of ω_r at $r = r_c - \frac{1}{4}d$ for twisting vortices at $Re = 2.186Re_c$, $a = 2.5$, $\beta = 135$.

Although undulating and twisting vortices are both travelling wave flows, they differ considerably. They may result from two different types of instability to non-axisymmetric disturbances. As just discussed, we propose that twisting waves result from a secondary shear instability. Using an inviscid analysis, a similar suggestion was made by Jones (1985) to explain the instability of Taylor vortex flow to wavy disturbances (see also Davey *et al.* 1968). However, twisting Dean vortex flow and wavy Taylor vortex flow are dissimilar, while undulating vortices and wavy Taylor vortices are similar. We suggest that undulating vortices and wavy Taylor vortices are due to a different type of instability than the one responsible for twisting vortex flow. To our knowledge, twisting vortices are not observed in the Taylor–Couette problem. Shear instability may not occur in Taylor–Couette flow, because the

streamwise shear layers are weaker than those in curved channel flow. This is a consequence of two factors: first, the shear layers have wider spacing in Taylor–Couette flow, i.e. experimental Taylor vortices have $\lambda \approx 2d$ compared to $\lambda \approx 1.25d$ for Dean vortices; second, the streamwise shear layers of both flows are caused by inflow/outflow between regions with large and small v_θ, but the radial separation of these regions is $\frac{1}{2}d$ in the channel as opposed to d in Taylor–Couette flow. Thus, for a given vortex strength, Dean vortices cause stronger streamwise shear layers.

Marcus (1984) postulates that wavy Taylor vortex flow is due to a secondary centrifugal instability that arises from the curvature of streamlines as they encircle a vortex centre. If we place a coordinate system (r', θ', z') at a vortex centre, with the (r', θ')-plane parallel to the (r, z)-plane, then Dean vortex flow streamlines, shown in figure 2, indicate that θ' angular momentum as a function of r' violates Rayleigh's stability criterion (4.1) at the inflow and outflow planes. A secondary centrifugal instability is a possible explanation for the development of undulating vortices; however, we have not produced any convincing evidence for such an instability mechanism. With both inner and outer cylinders rotating in the Taylor–Couette problem, far too many different flows occur (cf. Andereck, Liu & Swinney 1986) to be explained by one-dimensional secondary instability mechanisms. The instability responsible for undulating vortices and the many Taylor–Couette flows may be inherently two-/three-dimensional.

Marcus (1984) suggests that wavy Taylor vortices are due to a secondary centrifugal instability of the outflow boundaries and at higher Re the second travelling wave that occurs in modulated wavy vortex flow is due to a secondary centrifugal instability of the inflow boundaries. Because of the similarity of undulating vortices to wavy Taylor vortices, a modulated wavy Dean vortex flow occurring in the curved channel might be expected to be composed of two undulating waves. For sufficiently large Re, however, linear growth rates suggest that twisting waves predominate. Both inflow and outflow regions of twisting vortex flow could develop undulating waves via a secondary centrifugal instability mechanism. Based on the wavelength of undulating waves and wavy Taylor vortices, these would be long wavelength waves. The flows that occur in the curved channel with increasing Re before turbulence (chaos) occurs remain to be discovered.

9. Summary and conclusions

Curved channel flow provides an interesting geometry in which to examine instability and transition. Three-dimensional simulations of curved channel flow were used to study Dean vortices. Weakly nonlinear analysis of axisymmetric Dean vortices is accurate in only a limited range of Re and a. Linear stability analysis of non-axisymmetric disturbances shows that disturbances that are $\frac{1}{2}\pi$ out of phase (in the spanwise direction) with the axisymmetric vortices lead to wavy vortex flows. Spatial energy spectra for Dean vortex flow and wavy Dean vortices show exponential behaviour as a function of wavenumber. All flows studied obey shift-and-reflect symmetry to within roundoff error. Both axisymmetric and non-axisymmetric Dean vortices also show a vortex-doubling bifurcation, which may indicate the presence of an Eckhaus stability boundary. Such a boundary would limit the range of wavenumbers that can be observed experimentally.

Two distinct types of travelling wave flows arise: undulating and twisting Dean vortex flow. The angular speeds of travelling waves computed from linear theory are close to the actual speeds (even for large-amplitude waves), are only weakly

dependent on Re, a, β, and decrease with η. For the two η values examined, streamwise wavelengths of the most unstable travelling waves scale with the channel spacing. With increasing Re, disturbances with small streamwise wavenumbers become unstable first, producing an undulating vortex flow similar to wavy Taylor vortex flow. For $Re > Re''_{ns}$, a second type of instability occurs at shorter wavelengths and yields twisting Dean vortex flow as a consequence of a secondary shear instability. For $Re > Re''_{ns}$, axisymmetric vortices are unstable to both types of travelling waves, but no modulated wavy vortex flows were found for $Re < 8.199Re_c$. For $Re \gg Re''_{ns}$, linear growth rates associated with twisting vortices far exceed those associated with undulating vortices; therefore twisting vortices, not undulating vortices, should be observed at sufficiently high Re. Analysis indicates that full development of undulating vortices requires a streamwise distance greater than one circumference, while twisting vortices reach steady state within approximately πr_c when $Re > 2.5Re_c$ (for $\eta = 0.975$). Thus the undulating mode should be difficult to observe experimentally, while the twisting mode, whose existence in Taylor–Couette flow has not been demonstrated, should occur. Evidence for twisting vortex flow is found in the experiments of Kelleher *et al.* (1980) and Niver (1987).

In Taylor–Couette flow with $\eta = 0.875$, the transition to modulated wavy Taylor vortex flow is followed at higher Re by the development of weak turbulence, which is associated with a strange attractor (Brandstater & Swinney 1987). Turbulent Dean vortices have been observed by Moser & Moin (1984, 1987) at $Re \approx 20Re_c$ and by Hunt & Joubert (1979) at $Re \approx 125Re_c$. The route that curved channel flow follows between wavy Dean vortex flow and turbulent Dean vortices remains for future work.

The authors gratefully acknowledge NASA Ames Research Center for the use of their computing resources; this use was supported by the Air Force Office of Scientific Research under contract AF-84-0083. One of us (W.H.F.) would like to thank the Natural Sciences and Engineering Research Council of Canada and the Alberta Heritage Scholarship Fund for their financial support. The work of J.B.K. was supported by AFOSR, ONR and ARO.

Appendix

The equations for the eigenfunctions of §4 are derived as follows. Substituting (4.2) into the non-dimensional Navier–Stokes equations in cylindrical coordinates and making use of the equations obtained when $u = v = w = p' = 0$ yields

$$\left[\frac{1}{Re}\left(\mathrm{DD}^* + \frac{\partial^2}{\partial z^2}\right) - \frac{\partial}{\partial t}\right]u + \frac{2Vv}{r} - \mathrm{D}p' = u\,\mathrm{D}u + w\frac{\partial u}{\partial z} - \frac{v^2}{r}, \tag{A 1}$$

$$\left[\frac{1}{Re}\left(\mathrm{DD}^* + \frac{\partial^2}{\partial z^2}\right) - \frac{\partial}{\partial t}\right]v - u\left(\frac{\partial}{\partial r} + \frac{1}{r}\right)V - \frac{h_0}{r} = u\,\mathrm{D}v + w\frac{\partial v}{\partial z} + \frac{uv}{r}, \tag{A 2}$$

$$\left[\frac{1}{Re}\left(\mathrm{D}^*\mathrm{D} + \frac{\partial^2}{\partial z^2}\right) - \frac{\partial}{\partial t}\right)w - \frac{\partial p'}{\partial z} = u\,\mathrm{D}w + w\frac{\partial w}{\partial z}. \tag{A 3}$$

The continuity equation becomes

$$\mathrm{D}^*u + \frac{\partial w}{\partial z} = 0, \tag{A 4}$$

where we have defined $$\mathrm{D} \equiv \frac{\partial}{\partial r}, \quad \mathrm{D}^* \equiv \frac{\partial}{\partial r}+\frac{1}{r}. \tag{A 5}$$

The boundary conditions are

$$u = v = w = 0 \quad \text{at } r = r_\mathrm{i}, r_\mathrm{o}. \tag{A 6}$$

Substituting (4.5) into (A 1)–(A 4) we equate coefficients of $\cos naz$ and $\sin naz$, eliminate w_n by using the continuity equation, and eliminate p_n by using the third momentum equation. Performing the tedious algebra yields

$$\left(-\frac{\mathrm{DD}^*}{Re}+\frac{\partial}{\partial t}\right)v_0 = -\frac{h_0}{r}-\frac{1}{2}\left(\mathrm{D}^*+\frac{1}{r}\right)\sum_{n=1}^{\infty} nau_n v_n, \tag{A 7}$$

$$\left(\mathbf{L}_n+\frac{\partial}{\partial t}\mathbf{M}_n\right)\boldsymbol{Q}_n = \boldsymbol{S}_n(v_0, v_1, v_2, \ldots, u_1, u_2, \ldots), \quad n \geqslant 1, \tag{A 8}$$

where $\boldsymbol{Q}_n = (u_n, v_n)$, and $\boldsymbol{S}_n$ is a complicated quadratic function of u_i and v_i not given here because the final equations only require the first few terms of $\boldsymbol{S}_n$. The matrix differential operators $\mathbf{L}_n$ and $\mathbf{M}_n$ are

$$\left.\begin{aligned} \mathbf{L}_n &= \begin{pmatrix} \frac{1}{Re}(\mathrm{DD}^*-n^2a^2)^2 & -2naV/r \\ na\left(\frac{\partial V}{\partial r}+\frac{V}{r}\right) & -\frac{1}{Re}(\mathrm{DD}^*-n^2a^2) \end{pmatrix} \\ \mathbf{M}_n &= \begin{pmatrix} -(\mathrm{DD}^*-n^2a^2) & 0 \\ 0 & 1 \end{pmatrix} \end{aligned}\right\} \tag{A 9}$$

and the boundary conditions become

$$v_0 = 0, \quad u_n = v_n = \mathrm{D}u_n = 0 \quad \text{at } r = r_\mathrm{i}, r_\mathrm{o}, \quad n \geqslant 1. \tag{A 10}$$

Appropriate initial conditions for v_0, u_n, v_n are also necessary, but we shall seek only the steady-state solution, which is independent of these initial conditions. Equations (4.10), (4.12)–(4.15) follow by substituting (4.6)–(4.9) into (A 7) and (A 8).

As defined in §4, the first component of $\boldsymbol{S}_{20}$ is

$$\tfrac{1}{2}a\left\{u_{10}\left[\mathrm{D}^3u_{10}-\frac{\mathrm{D}^2u_{10}}{r}-\frac{3}{r^2}\mathrm{D}u_{10}+\left(2a^2+\frac{4}{r^2}\right)\frac{u_{10}}{r}\right]-\mathrm{D}u_{10}\,\mathrm{D}^2u_{10}-\frac{(\mathrm{D}u_{10})^2}{r}+\frac{2}{r}v_{10}^2\right\},$$

and the second component is

$$\tfrac{1}{2}a(v_{10}\,\mathrm{D}u_{10}-u_{10}\,\mathrm{D}v_{10}).$$

The first component of $\boldsymbol{S}_{13}$ is

$$\begin{aligned} a\Big[&\frac{1}{r}v_{10}v_{20}+\frac{2}{r}v_{00}v_{10}+\frac{1}{2}u_{10}\,\mathrm{D}^3u_{20}+\mathrm{D}u_{10}\,\mathrm{D}^2u_{20} \\ &+\frac{1}{r}u_{10}\,\mathrm{D}^2u_{20}-\frac{1}{2}\mathrm{D}^2u_{10}\,\mathrm{D}u_{20}+\frac{1}{2r}\mathrm{D}u_{10}\,\mathrm{D}u_{20}-\frac{3}{2}a^2u_{10}\,\mathrm{D}u_{20} \\ &-u_{20}\,\mathrm{D}^3u_{10}-\frac{1}{2r}\mathrm{D}^2u_{10}u_{20}+\frac{3}{2r^2}u_{20}\mathrm{D}u_{10}-3a^2u_{20}\,\mathrm{D}u_{10}-u_{10}\,u_{20}\left(\frac{2}{r^3}+\frac{5a^2}{2r}\right)\Big], \end{aligned}$$

and the second component is

$$-a\left(\frac{1}{2}u_{10}\,\mathrm{D}v_{20}+v_{20}\,\mathrm{D}u_{10}+\frac{3}{2r}u_{10}v_{20}+u_{20}\,\mathrm{D}v_{10}\right.$$
$$\left.+\frac{1}{2}v_{10}\,\mathrm{D}u_{20}+\frac{3}{2r}u_{20}v_{10}+u_{10}\,\mathrm{D}v_{00}+\frac{1}{r}u_{10}v_{00}\right).$$

REFERENCES

Ahlers, G., Cannell, D. S. & Dominguez-Lerma, M. A. 1983 Possible mechanism for transitions in wavy Taylor-vortex flow. *Phys. Rev.* A **27**, 1225–1227.

Andereck, C. D., Liu, S. S. & Swinney, H. L. 1986 Flow regimes in a circular Couette system with independently rotating cylinders. *J. Fluid Mech.* **164**, 165–183.

Bennett, J. & Hall, P. 1986 On the secondary instability of Taylor–Görtler vortices to Tollmien–Schlichting waves in fully developed flows. *NASR CR* 178221.

Berger, S. A., Talbot, L. & Yao, L.-S. 1983 Flow in curved pipes. *Ann. Rev. Fluid Mech.* **15**, 461–512.

Bippes, H. 1978 Experimental study of the laminar–turbulent transition of a concave wall in a parallel flow. *NASA TM* 75243.

Brandstater, A. & Swinney, H. L. 1987 Strange attractors in weakly turbulent Couette–Taylor flow. *Phys. Rev.* A **35**, 2207–2220.

Brewster, D. B., Grosberg, P. & Nissan, A. H. 1959 The stability of viscous flow between horizontal concentric cylinders. *Proc. R. Soc. Lond.* A **251**, 76–91.

Cheng, K. C. & Akiyama, M. 1970 Laminar forced convection heat transfer in curved rectangular channels. *Intl J. Heat Mass Transfer* **13**, 471–490.

Cheng, K. C., Lin, R-C. & Ou, J-W. 1976 Fully developed laminar flow in curved rectangular channels. *Trans. ASME* I: *J. Fluids Engng* **98**, 41–48.

Daudpota, Q. I., Zang, T. A. & Hall, P. 1987 Interaction of Görtler vortices and Tollmien–Schlichting waves in curved channel flow. *AIAA Paper* 87-1205.

Davey, A. 1962 The growth of Taylor vortices in flow between rotating cylinders. *J. Fluid Mech.* **14**, 336–368.

Davey, A., DiPrima, R. C. & Stuart, J. T. 1968 On the instability of Taylor vortices. *J. Fluid Mech.* **31**, 17–52.

Dean, W. R. 1928 Fluid motion in a curved channel. *Proc. R. Soc. Lond.* A **121**, 402–420.

DiPrima, R. C. 1967 Vector eigenfunction expansions for the growth of Taylor vortices in the flow between rotating cylinders. In *Nonlinear Partial Differential Equations* (ed. W. F. Ames), pp. 19–42. Academic.

DiPrima, R. C. & Swinney, H. L. 1985 Instabilities and transition in flow between concentric rotating cylinders. In *Hydrodynamic Instabilities and the Transition to Turbulence*, 2nd edn (ed. H. L. Swinney & J. P. Gollub), Topics in Applied Physics, vol. 45, pp. 139–180. Springer.

Dominguez-Lerma, M. A., Cannell, D. S. & Ahlers, G. 1986 Eckhaus boundary and wave-number selection in rotating Couette–Taylor flow. *Phys. Rev.* A **34**, 4956–4970.

Drazin, P. G. & Reid, W. H. 1981 *Hydrodynamic Stability.* Cambridge University Press.

Fenstermacher, P. R., Swinney, H. L. & Gollub, J. P. 1979 Dynamical instabilities and the transition to chaotic Taylor vortex flow. *J. Fluid Mech.* **94**, 103–128.

Finlay, W. H., Keller, J. B. & Ferziger, J. H. 1987*a* Instability and transition in curved channel flow. *Rep. TF-30*, Dept. of Mech. Eng., Stanford University, CA.

Finlay, W. H., Keller, J. B. & Ferziger, J. H. 1987*b* Finite amplitude vortices in curved channel flow. *AIAA Paper* 87-0363.

Flentie, D. L. 1975 An experimental study of Taylor–Goertler vortices in a curved rectangular channel. M.S. thesis, Naval Postgraduate School, Monterey, CA.

Gibson, R. D. & Cook, A. E. 1974 The stability of curved channel flow. *Q. J. Mech. Appl. Maths* **27**, 149–160.

GOLLUB, J. P. & FRIEDLICH, M. H. 1976 Optical heterodyne test of perturbation expansions for the Taylor instability. *Phys. Fluids* **19**, 618–626.

HAMMERLIN, G. 1958 Die Stabilität der Strömung in einem gekrümmten Kanal. *Arch. Rat. Mech. Anal.* **1**, 212–224.

HUNT, I. A. & JOUBERT, P. N. 1979 Effects of small streamline curvature on turbulent duct flow. *J. Fluid Mech.* **91**, 633.

IOOSS, G. 1986 Secondary bifurcations of Taylor vortices into wavy inflow or outflow boundaries. *J. Fluid Mech.* **173**, 273–288.

JANKOWSKI, D. F. & TAKEUCHI, D. I. 1976 The energy stability limit for flow in a curved channel. *Trans. ASME* E: *J. Appl. Mech.* **43**, 1–3.

JONES, C. A. 1981 Nonlinear Taylor vortices and their stability. *J. Fluid Mech.* **102**, 249–261.

JONES, C. A. 1985 The transition to wavy Taylor vortices. *J. Fluid Mech.* **157**, 135–162.

JOSEPH, B., SMITH, E. P. & ADLER, R. J. 1975 Numerical treatment of laminar flow in helically coiled tubes of square cross-section. Part 1. Stationary helically coiled tubes. *AIChE J.* **21**, 965–974.

KELLEHER, M. D., FLENTIE, D. L. & MCKEE, R. J. 1980 An experimental study of the secondary flow in a curved rectangular channel. *Trans. ASME* I: *J. Fluids Engng* **102**, 92–96.

KELLER, H. B. 1977 Numerical solution of bifurcation and nonlinear eigenvalue problems. In *Applications of Bifurcation Theory*, pp. 359–384. Academic.

KING, G. P., LI, Y., LEE, W., SWINNEY, H. L. & MARCUS, P. S. 1984 Wave speeds in wavy Taylor vortex flow. *J. Fluid Mech.* **141**, 365.

KING, G. P. & SWINNEY, H. L. 1983 Limits of stability and irregular flow patterns in wavy vortex flow. *Phys. Rev.* A **27**, 1240–1243.

KOGELMAN, S. & DIPRIMA, R. C. 1970 Stability of spatially periodic supercritical flows in hydrodynamics. *Phys. Fluids* **13**, 1–11.

MARCUS, P. S. 1984 Simulation of Taylor–Couette flow. Part 2. Numerical results for wavy-vortex flow with one travelling wave. *J. Fluid Mech.* **146**, 65–113.

MASLOWE, S. A. 1985 Shear flow instabilities and transition. In *Hydrodynamic Instabilities and the Transition to Turbulence*, 2nd edn (ed. H. L. Swinney & J. P. Gollub), Topics in Applied Physics, vol. 45, pp. 181–278. Springer.

MCKEE, R. J. 1973 An experimental study of Taylor–Goertler vortices in a curved rectangular channel. Engineer's thesis, Naval Postgraduate School, Monterey, CA.

MEYER-SPASCHE, R. & KELLER, H. B. 1985 Some bifurcation diagrams for Taylor vortex flows. *Phys. Fluids* **28**, 1248–1252.

MOSER, R. D. & MOIN, P. 1984 Direct numerical simulation of curved turbulent channel flow. *NASA TM* 85974.

MOSER, R. D. & MOIN, P. 1987 The effects of curvature in wall-bounded turbulent flow. *J. Fluid Mech.* **175**, 497–510.

MOSER, R. D., MOIN, P. & LEONARD, A. 1983 A spectral numerical method for the Navier–Stokes equations with applications to Taylor–Couette flow. *J. Comp. Phys.* **52**, 524–544.

NAYFEH, A. H. 1987 Nonlinear stability of boundary layers. *AIAA Paper* 87-0044.

NIVER, R. D. 1987 Structural characteristics of Dean vortices in a curved channel. M.Sc. thesis, Naval Postgraduate School, Monterey, CA.

RAND, D. 1982 Dynamics and Symmetry. Predictions for modulated waves in rotating fluids. *Arch. Rat. Mech. Anal.* **79**, 1–37.

RAYLEIGH, J. W. S. 1916 On the dynamics of revolving fluids. *Proc. R. Soc. Lond.* A **93**, 148–154.

REID, W. H. 1958 On the stability of viscous flow in a curved channel. *Proc. R. Soc. Lond.* A **244**, 186–198.

RIECKE, H. & PAAP, H. 1986 Stability and wave-vector restriction of axisymmetric Taylor vortex flow. *Phys. Rev.* A **33**, 547–553.

SCHILLING, R. & SIMON, R. 1979 Berechnung der ausgebildeten Strömung in gekrümmten Kanälen mit rechteckigem Querschnitt. In *Recent Developments in Theoretical and Experimental Fluid Mechanics* (ed. U. Müller, K. G. Roesner & B. Schmidt), pp. 546–556. Springer.

SINGER, B. A., FERZIGER, J. H. & REED, H. L. 1987 Effect of streamwise vortices on transition in plane-channel flow. *AIAA Paper* 87-0048.

SHANTHINI, W. & NANDAKUMAR, K. 1986 Bifurcation phenomena of generalized Newtonian fluids in curved rectangular ducts. *J. Non-Newtonian Fluid Mech.* **22**, 35–60.

SPARROW, E. M. 1964 On the onset of flow instability in a curved channel of arbitrary height. *Z. Angew. Math. Phys.* **15**, 638–642.

STUART, J. T. 1960 On the non-linear mechanics of wave disturbances in stable and unstable parallel flows. Part 1. The basic behaviour in plane Poiseuille flow. *J. Fluid Mech.* **9**, 353–370.

STUART, J. T. 1986 Taylor–Vortex flow: a dynamical system. *SIAM Rev.* **28**, 315–342.

WALOWIT, J., TSAO, S. & DIPRIMA, R. 1964 Stability of flow between arbitrarily spaced concentric cylindrical surfaces including the effect of a radial temperature gradient. *Trans. ASME* E. *J. Appl. Mech.* **31**, 585–593.

WATSON, J. 1960 On the non-linear mechanics of wave disturbances in stable and unstable parallel flows. Part 2. The development of a solution for plane Poiseuille flow and for plane Couette flow. *J. Fluid Mech.* **9**, 371–389.

WINTERS, K. H. 1987 A bifurcation study of laminar flow in a curved tube of rectangular cross-section. *J. Fluid Mech.* **180**, 343–369.